

CGC predictions for p+Pb collisions at the LHC

Javier L. Albacete^a, Adrian Dumitru^b, Hirotugu Fujii^c and Yasushi Nara^d

^a*IPNO, Université Paris-Sud 11, CNRS/IN2P3, 91406 Orsay, France*

^b*Department of Natural Sciences, Baruch College, CUNY, 17 Lexington Avenue, New York, NY 10010, USA*

RIKEN BNL Research Center, Brookhaven National Laboratory, Upton, NY 11973, USA

^c*Institute of Physics, University of Tokyo, Komaba, Tokyo 153-8902, Japan*

^d*Akita International University, Yuwa, Akita-city 010-1292, Japan*

We present predictions for multiplicities and single inclusive particle production in proton-lead collisions at the LHC. The main dynamical input in our calculations is the use of solutions of the running coupling Balitsky-Kovchegov equation tested in e+p data. These are incorporated into a realistic model for the nuclear geometry including fluctuations of the nucleon configurations. Particle production is computed via either k_t -factorization or the *hybrid* formalisms to obtain spectra and yields in the central and forward rapidity regions, respectively. These baseline predictions will be useful for testing our current understanding of the dynamics of very strong color fields against upcoming LHC data.

I. INTRODUCTION

Heavy-ion collision programs performed previously at the RHIC and SPS accelerators have always benefited tremendously from insight obtained by proton (deuteron)-nucleus collisions. It is expected, also, that the planned p+Pb run at the LHC will provide crucial benchmarks for the characterization of the hot QCD medium produced in lead-lead collisions, arguably a Quark Gluon Plasma (QGP). The absence of intricate final state effects induced by the formation of a QGP renders proton-nucleus collisions an excellent laboratory to study the so called initial state effects. These originate from the fact that the colliding nuclei do not behave as a mere incoherent superposition of their constituent nucleons. Rather, coherence effects are important and modify not only the partonic flux into the collision, but also the underlying dynamics of particle production in the scattering processes. A careful distinction of initial from final state effects is of vital importance for a proper characterization of the latter, as they may lead sometimes to qualitatively similar phenomena in observables of interest. Physics prospects for the p+Pb at the LHC run were recently compiled in [1].

Besides its role as a reference experiment, the p+Pb run at the LHC will provide access to kinematic regions never explored so far in nuclear collisions and thus carries great potential for discovery of new QCD phenomena on its own. In particular, the huge leap forward in collision energy with respect to previous high energy electron-nucleus or proton-nucleus experiments¹ will probe the nuclear wave function at values of Bjorken- x smaller than ever before. It is theoretically well established that at small enough values of Bjorken- x QCD enters a novel regime governed by large gluon densities and non-linear coherence phenomena [2]. The Color Glass Condensate (CGC) effective theory provides a consistent framework to study QCD scattering at small- x or high collision energies (for a review see e.g. [3, 4]). It is based on three main physical ingredients: First, high gluon densities correspond to strong classical fields [5, 6], which permit ab-initio first principles calculation of “wave functions” at small x through classical techniques. Next, quantum corrections are incorporated via non-linear renormalization group equations such as the B-JIMWLK hierarchy or, in the large- N_c limit, the BK equation [7, 8] which describe the evolution of the hadron wave function towards small x . The non-linear, density-dependent terms in the CGC evolution equations are ultimately related to unitarity of the theory and, in the appropriate frame and gauge, can be interpreted as due to gluon recombination processes that tame or *saturate* the growth of gluon densities for modes with transverse momenta below a dynamically generated scale known as the saturation scale, $Q_s(x)$. Finally, the presence of strong color fields $\mathcal{A} \sim 1/g$ leads to breakdown of standard perturbative techniques to describe particle production processes based on a series expansion in powers of the strong coupling g . Terms of order $g\mathcal{A} \sim \mathcal{O}(1)$ need to be resummed to all orders. The CGC provides the tools to perform such resummation although the precise prescription for the resummation may vary from process to process or colliding system.

An important step towards promoting the CGC to a practical phenomenological tool has been performed recently through the calculation of higher order corrections to the BK-JIMWLK equations [9–12]. In particular,

¹ The expected center of mass collision energy for the p+Pb run is 5 TeV, to be compared to a maximal energy of 200 GeV for RHIC d+Au collisions.

the calculation of running coupling corrections to the evolution kernel of the BK equation (referred to as rcBK henceforth) made it possible to describe various data at high energies in terms of solutions of the rcBK equation, thus closing the gap between first principles theory calculations and data [13].

Despite the fact that CGC effects are expected to be enhanced in nuclei versus protons, which is due to the larger valence charge densities per unit transverse area in nuclei, so far the most exhaustive searches of the saturation phenomenon have been performed using data on proton reactions. This is mainly due to the large body of high quality DIS data on protons at small- x . Thus, the global fits performed by the AAMQS collaboration in [14–16] demonstrated that the rcBK equation successfully accounts for the x -dependence of inclusive structure functions measured in electron-proton collisions at HERA at small- x (see also [17] for fits to diffractive data). Here, we shall use the resulting AAMQS parametrizations of the dipole-proton scattering amplitude as a basic building block for the nuclear unintegrated distributions. Furthermore, as discussed in more detail below, single inclusive p_\perp spectra in proton+proton collisions at Tevatron, LHC and forward RHIC data are well described in the CGC framework [18–20]. In case of heavy-ion collisions, the most compelling indications of CGC effects in data are due to suppression phenomena observed at RHIC d+Au collisions in the forward rapidity region. Actually, single particle distributions in both p+p and d+Au collisions and the depletion of nuclear modification factors R_{dAu} were well described by CGC calculations in [18, 19]. However, forward RHIC data are close to the kinematic limit of phase space, probing the projectile wave function at large values of $x \rightarrow 1$ and the fragmentation functions at $z \rightarrow 1$. This allows for alternative descriptions of the data based on large- x phenomena such as energy loss [21]. A clearer signal of gluon saturation is provided by the observed disappearance of back-to-back di-hadron correlations in d+Au collisions. CGC calculations predicted first [22], and later on quantitatively accounted for [23, 24], such suppression. The disappearance of the away-side peak can be understood in terms of multiple scatterings controlled by a dynamical transverse scale, the saturation scale of the nucleus. Even though no description of such data that does not invoke saturation effects is known to date (see however [25]), it has been argued that large- x effects like energy loss or enhancement of double scattering processes may blur the interpretation of angular decorrelation between hadron pairs as due to CGC effects [26]. Additionally, the good description of the energy and centrality dependence of integrated multiplicities in RHIC Au+Au and d+Au collisions and in Pb+Pb collisions at the LHC in CGC models lends further support to the idea that saturation effects are relevant in present data, although the larger degree of modeling involved in their calculation prevents making any definite claims. In summary, although it may be argued that the present data do not provide sharp and direct evidence for neither the saturation regime of QCD nor the CGC approach to saturation, it is fair to say that HERA, RHIC and available LHC data lead to a rather coherent picture, with several phenomena finding their natural interpretation in terms of high density gluonic systems together with a consistent quantitative description in the CGC framework at its present degree of accuracy.

Regardless of the question whether the CGC is the most suited framework for their description there is broad consensus that coherence effects are important for the interpretation of present data on heavy ion collisions. In fact most –if not all– of the different phenomenological approaches for the description of particle production –both in the soft or hard sector– include physical ingredients related to either the depletion of gluon content of nuclei (e.g. the leading twist shadowing of the nuclear parton distributions in the collinear factorization formalism or string fusion processes in Dual Parton or percolation models), the breakdown of independent particle production from the individual participant nucleons (e.g. through the presence of energy dependent cut-offs in event generators like HIJING or HYDJET) or effective resummations of multiple scatterings². All these ingredients are akin, at least at a conceptual level, to those dynamically built in the CGC, although they are formulated in very different ways.

The p+Pb run at the LHC will provide an excellent –and probably in the near future unique– possibility to disentangle the presently inconclusive situation on the role of CGC effects and also to distinguish among different approaches to describe high energy scattering in nuclear collisions. On the one hand, the LHC shall bring us closer to the limit of asymptotically high energy in which the CGC formalism is developed, thus reducing theoretical uncertainties on its applicability. Equivalently, the value of the saturation scale is expected to be a factor $\sim 2 \div 4$ times larger than at RHIC, so saturation effects should be visible in a larger range of transverse momenta, deeper into the perturbative domain. On the other hand, the much extended energy reach of the LHC will allow measurements far from the kinematic limit up to very forward rapidities, thus minimizing the role of large- x effects which obscured the interpretation of forward RHIC data.

Although more exclusive observables like di-hadron or hadron-photon correlations are expected to better discriminate between different approaches, a first test for models of particle production shall come from data on

² Here we just mention a few well known examples; a rather exhaustive compilation of phenomenological works for the description of particle production in HIC can be found in e.g. [27].

inclusive multiplicities and single particle distributions as they are much easier to obtain experimentally. In this work we aim to provide up-to-date predictions for these observables within the framework of the running coupling BK Monte Carlo (rcBK-MC) previously presented in [28] and built as an upgrade of the original KLN-MC code [29]. The rcBK-MC model presented here attempts to incorporate up-to-date tools on the CGC theoretical side, namely the use of solutions of the rcBK equation as main dynamical input to describe the x and transverse momentum dependence of nuclear unintegrated gluon distributions, combined with the empiric information gained from the analysis of e+p, p+p and RHIC nuclear collisions. The Monte Carlo treatment allows for a realistic treatment of the collision geometry including in particular realistic nuclear density distributions as well as fluctuations of the configurations of nucleons. This is important in order to obtain the number of collisions N_{coll} used in the definition of the nuclear modification factor R_{pA} consistently with the computed p+A spectra, within one single framework. Also, fluctuations of the number of target nucleons are particularly relevant for particle production in the high density regime where the number of small- x gluons is not linearly proportional to the number of valence charges.

There are two distinct but related approaches to hadron production in high energy asymmetric (such as proton-nucleus or very forward proton-proton and nucleus-nucleus) collisions. In such collisions, particle production processes in the central rapidity region probe the wave functions of both projectile and target at small values of x . Here, one may employ the k_t -factorization formalism where both the projectile and target are characterized in terms of their rcBK evolved unintegrated gluon distributions (UGDs).

At more forward rapidities, on the other hand, the proton is probed at larger values of x while the target nucleus is shifted deeper into the small- x regime. Here, k_t -factorization fails to grasp the dominant contribution to the scattering process. Rather, the *hybrid* formalism proposed in ref. [30] and embedded recently in a Monte Carlo treatment of the nuclear geometry [19, 20] is more appropriate. In the hybrid formalism the large- x degrees of freedom of the proton are described in terms of usual parton distribution functions (PDFs) of collinear factorization which satisfy the momentum sum rule exactly and which exhibit a scale dependence given by the DGLAP evolution equations. On the other hand, the small- x glue of the nucleus is still described in terms of its UGD. Recently the hybrid formalism has been improved through the calculation of inelastic contributions that may become important at high transverse momentum [31]. We shall investigate the effect of this new production channel in our predictions. Unfortunately, no smooth matching between the k_t -factorization and *hybrid* formalisms is known to date. Also, their corresponding limits of applicability –equivalently the precise value of x at which one should switch from one to the other– have only been estimated on an empirical basis. We shall explore the stability of CGC predictions using one or the other formalism as one varies the kinematics of the detected hadron.

One important goal of this work is to systematically assess the model (and implementation) uncertainties. Such calibration is mandatory in order to actually prove or disprove different approaches by comparison to data. This is specially so in the case of semi-inclusive observables such as the ones discussed in this work where “only” quantitative differences arise between predictions from different approaches (contrary to the case of more exclusive observables).

In the rcBK-MC model presented here, uncertainties originate from either the modeling of non-perturbative aspects of the collision or from high-order corrections to fixed order perturbative calculations for particle production. Among the former are the initial conditions for rcBK evolution, which are only partially constrained by global fits to e+p data, or modeling of the impact parameter dependence of the nuclear UGDs. Perturbative tools such as the rcBK equation are ill-suited to provide a simultaneous, unified description of both the Bjorken- x and impact parameter dependence of the UGD of a nucleus (or any other hadron) since the latter is related to the physics of confinement. This makes some degree of modeling unavoidable. Concerning the uncertainties due to fixed order perturbative calculations, they are either absorbed in K -factors or explored through the variation of factorization and running coupling scales. The K -factors discussed here should also absorb effects not included in the CGC approach.

II. THE NUCLEAR UNINTEGRATED GLUON DISTRIBUTIONS

The paucity of small- x data with nuclei prevents a direct empiric determination of the nuclear unintegrated gluon distribution at small- x . Here we shall build the nuclear UGD entirely from the nucleon UGD extracted by the AAMQS collaboration through global fits to inclusive e+p data on structure functions.

Before proceeding further, let us briefly recall the basic features of the AAMQS approach. The main dynamical ingredient is the dipole formulation of deep inelastic scattering (DIS). The AAMQS fits rely upon is the $q\bar{q}$ dipole scattering amplitude off a hadron, $\mathcal{N}_F(r, x, \mathbf{R})$, where x is the usual Bjorken scaling variable in DIS, r is the dipole transverse size and \mathbf{R} the transverse position at which the hadron target is probed. The index F refers to the fact that the dipole constituents –quark and antiquark– belong to the fundamental representation of $SU(3)$. In the

large N_c -limit the B-JIMWLK equations reduce to a single, closed equation for the x -dependence of the dipole amplitude, which is the so-called BK equation. Under the assumption of translational invariance implicit in the AAMQS approach, and hence omitting the \mathbf{R} -dependence of the dipole amplitude accordingly, the BK equation including running coupling corrections (referred to as rcBK in what follows) reads

$$\frac{\partial \mathcal{N}_F(r, x)}{\partial \ln(x_0/x)} = \int d^2 \underline{r}_1 K^{run}(\underline{r}, \underline{r}_1, \underline{r}_2) [\mathcal{N}_F(r_1, x) + \mathcal{N}_F(r_2, x) - \mathcal{N}_F(r, x) - \mathcal{N}_F(r_1, x) \mathcal{N}_F(r_2, x)] \quad (1)$$

where $\mathbf{r} = \mathbf{r}_1 + \mathbf{r}_2$ ³ and K^{run} is the evolution kernel including running coupling corrections:

$$K^{run}(\mathbf{r}, \mathbf{r}_1, \mathbf{r}_2) = \frac{N_c \alpha_s(r^2)}{2\pi^2} \left[\frac{1}{r_1^2} \left(\frac{\alpha_s(r_1^2)}{\alpha_s(r_2^2)} - 1 \right) + \frac{r^2}{r_1^2 r_2^2} + \frac{1}{r_2^2} \left(\frac{\alpha_s(r_2^2)}{\alpha_s(r_1^2)} - 1 \right) \right]. \quad (2)$$

In practical implementations, the running coupling in Eq. (2) is regularized in the infrared by freezing it to a constant value $\alpha_{fr} = 0.7$.

Solving the BK equation is an initial value problem, i.e. it is well defined only after initial conditions at the initial evolution scale, $x_0 = 10^{-2}$ in the AAMQS fits, and for all values of the dipole size r have been provided. This introduces free parameters, ultimately of non-perturbative origin, to be fitted to data. In the AAMQS rcBK fits to HERA data the initial conditions are taken in the form

$$\mathcal{N}_F(r, x=x_0) = 1 - \exp \left[- \frac{(r^2 Q_{s0,proton}^2)^\gamma}{4} \ln \left(\frac{1}{\Lambda r} + e \right) \right], \quad (3)$$

where $\Lambda = 0.241$ GeV, $Q_{s0,proton}^2$ is the saturation scale at the initial scale x_0 and γ is a dimensionless parameter that controls the steepness of the tail of the unintegrated gluon distribution for momenta above the saturation scale $k_t > Q_{s0,proton}$. Both $Q_{s0,proton}^2$ and γ are fitted to data. Although the AAMQS fits clearly favor values $\gamma > 1$, they do not uniquely determine its optimal value (and neither does the analysis of forward RHIC data performed in ref. [19]). Rather, different pairs of $(Q_{s0,proton}^2, \gamma)$ parameters provide comparable values of $\chi^2/\text{d.o.f} \sim 1$. The reason for this behavior is that they are correlated with other parameters, such as the overall normalization of the γ^* -p cross section, and also that HERA data is too inclusive to constrain exclusive features of the proton UGD. In order to account for such uncertainty we shall consider two of the AAMQS sets, corresponding to $(Q_{s0,proton}^2, \gamma) = (0.168 \text{ GeV}^2, 1.119)$ and $(0.157 \text{ GeV}^2, 1.101)$. Additionally, we shall also consider the McLerran Venugopalan (MV) model [5, 6] which corresponds to Eq. (3) with $\gamma = 1$; the MV model is well established theoretically (for very large nuclei, $gA^{1/3} \gg 1$) and has been used frequently in the literature. We note that $\gamma > 1$ for the proton may arise from corrections to the effective action of the MV model of higher order in the valence color charge density [32]. Such corrections are expected to decrease with increasing nuclear thickness. Therefore, it is conceivable that the dipole-nucleus scattering amplitude may be better represented by the MV model than by initial conditions with $\gamma > 1$. However, using the AAMQS ($\gamma > 1$) i.c. for the proton simultaneously with an MV i.c. for the nucleus leads to a monotonical increase (with p_t) of the nuclear modification factor R_{pPb} which is due to the different power-law fall off of the respective UGDs. We shall not study this option in detail in this work. Also, we recall that in the AAMQS fits the strong coupling is evaluated according to the following expression:

$$\alpha_s(r^2) = \frac{4\pi}{\beta \ln \left(\frac{4C^2}{r^2 \Lambda^2} + \mu \right)} \quad (4)$$

where $\beta = 11 - \frac{2}{3}N_f$, $N_f = 3$, $\Lambda = 0.241$ GeV and the constant C under the logarithm accounts for the uncertainty inherent to the Fourier transform from momentum space, where the original calculation was performed. A parameter μ is introduced to regulate the strong coupling for large dipole sizes, and fixed by the condition $\alpha_s(\infty) = \alpha_{fr}$. The $(Q_{s0,proton}^2, \gamma, \alpha_{fr}, C)$ -values considered here are shown in Table I.

UGD Set	$Q_{s0,proton}^2$ (GeV ²)	γ	α_{fr}	C
MV	0.2	1	0.5	1
g1.119	0.168	1.119	1.0	2.47
g1.101	0.157	1.101	0.8	1

TABLE I: Summary of parameters for the three dipole-proton scattering amplitudes (or UGDs) considered in this work.

³ We use the notation $v \equiv |\mathbf{v}|$ for two-dimensional vectors throughout the paper.

In the large- N_c limit the gluon dipole scattering amplitude required for the unintegrated gluon distributions can be obtained from the quark dipole scattering amplitude that solves the rcBK equation:

$$\mathcal{N}_A(r, x, \mathbf{R}) = 2\mathcal{N}_F(r, x, \mathbf{R}) - \mathcal{N}_F^2(r, x, \mathbf{R}) \quad (5)$$

where the subscript A simply refers to the fact that gluons belong to the adjoint representation of $SU(3)$. Note that this relation entails that the saturation momentum relevant for gluon scattering is larger than that for quark scattering by about a factor of 2, at the initial rapidity $x = x_0$.

The nuclear UGDs needed for particle production in the k_t -factorization and *hybrid* frameworks are related to the quark and gluon dipole scattering amplitudes via 2-dimensional Fourier transforms. In particular, the UGD entering the k_t -factorization formula is given by

$$\varphi(k, x, \mathbf{R}) = \frac{C_F}{\alpha_s(k) (2\pi)^3} \int d^2\mathbf{r} e^{-i\mathbf{k}\cdot\mathbf{r}} \nabla_{\mathbf{r}}^2 \mathcal{N}_A(r, x, \mathbf{R}). \quad (6)$$

The function φ is dimensionless and corresponds to the number of gluons per unit transverse area and per transverse momentum space cell.

Eq. (6) was written originally for fixed coupling. In order to be consistent with our treatment of the small- x evolution, we have extended it by allowing the coupling in the denominator to run with the momentum scale. As explained in [28], this modification turns out to be important to obtain a good description of the centrality dependence of the charged hadron multiplicities measured in Au+Au and Pb+Pb collisions at RHIC and the LHC respectively, which are otherwise too flat. In turn, the following UGDs in the fundamental and adjoint representations are needed in the *hybrid* framework:

$$\tilde{\mathcal{N}}_{F(A)}(k, x, \mathbf{R}) = \int d^2\mathbf{r} e^{-i\mathbf{k}\cdot\mathbf{r}} [1 - \mathcal{N}_{F(A)}(r, x, \mathbf{R})] \quad (7)$$

Note that although the AAMQS approach assumes translational invariance –i.e. impact parameter independence– of the dipole scattering amplitude over transverse distances of the order of the nucleon radius, R_N , we have made explicit such dependence in equations Eqs. (5-7) for consistency with the notation employed for nuclear UGDs where the impact parameter dependence must be considered.

Let us now discuss our model for the nuclear UGD, starting from the one for a nucleon⁴. First, we assume that the functional form of the quark dipole scattering amplitude off a nucleus at the initial saturation scale $x = x_0 = 0.01$ is the same as for the quark dipole scattering amplitude off a proton but with a shifted initial saturation scale that depends on the local density at every point in the transverse plane, \mathbf{R} . In other words, we shall replace

$$Q_{s0,\text{proton}}^2 \rightarrow Q_{s0,\text{nucleus}}^2(\mathbf{R}) \quad (8)$$

in Eq. (3) in order to define the initial conditions for the evolution of the quark dipole scattering off a nucleus at every transverse point in the nucleus. Then, the initial conditions given by Eqs. (3) and (8) are evolved locally using the impact parameter independent rcBK evolution defined by Eqs. (1-2). This provides the full (r, x) -dependence of the quark dipole-nucleus scattering amplitude at every point in the transverse plane of the nucleus. Finally, Eqs. (6-7) are used to calculate their Fourier transform which provide the complete transverse momentum k_t , Bjorken- x and impact parameter (\mathbf{R}) dependence of the nuclear UGDs.

To complete our discussion of the initial conditions we explain how we construct $Q_{s0,\text{nucleus}}^2(\mathbf{R})$. We treat the transverse positions of nucleons as random variables following a two-dimensional projection of the Woods-Saxon distribution, $T_A(\mathbf{R})$. Each configuration consist of a list of random coordinates \mathbf{r}_i , $i = 1 \dots A$, for the locations of the different nucleons in the transverse plane; A denotes the atomic mass number of the nucleus. Multi-nucleon correlations are neglected except for imposing a short-distance hard core repulsion which enforces a minimal distance ≈ 0.4 fm between any two nucleons.

Every such configuration defines a different local density in the transverse plane of the nucleus. Obviously, the smallest non-zero local density corresponds to the presence of a single nucleon. On the other hand, rare fluctuations where a large number of nucleons is encountered at a given transverse position can occur. Such configurations correspond to a high initial saturation scale, $Q_{s0,\text{nucleus}}^2(\mathbf{R})$. For a given configuration, the initial saturation

⁴ Strictly speaking, the AAMQS fits provide information only on the proton UGD or dipole scattering amplitude. We shall assume that isospin effects are negligible for the gluon distributions at small- x and consider it equal to the one of a neutron.

momentum $Q_{s0,\text{nucleus}}^2(\mathbf{R})$ at the transverse coordinate \mathbf{R} is taken to be proportional to the local variance of the density of valence charges which is itself proportional to the number of overlapping nucleons at that transverse point, $N(\mathbf{R})$:

$$a) \quad Q_{s0,\text{nucleus}}^2(\mathbf{R}) = N(\mathbf{R}) Q_{s0,\text{proton}}^2. \quad (9)$$

We shall refer to this option as *natural* in what follows. Note that these valence charge sources generate the small- x gluon fields described by the UGD *coherently*. For the AAMQS initial condition, the prescription (9) may lead to an inconsistent definition of the nuclear modification factor in the limit of large transverse momentum because additivity of the dipole scattering amplitude in the number of nucleons, $\mathcal{N}(r; x_0, \mathbf{R}) \sim T_A(\mathbf{R})$ at small r , is violated. To fix this issue we shall also consider a second possibility to generate $Q_{s0,\text{nucleus}}^2(\mathbf{R})$:

$$b) \quad Q_{s0,\text{nucleus}}^2(\mathbf{R}) = N(\mathbf{R})^{1/\gamma} Q_{s0,\text{proton}}^2, \quad (10)$$

where γ is one of the parameters in the initial condition, see Eq. (3). This *ansatz* –to which we shall refer as *modified*– is motivated by the requirement that nuclear modification factors should go to unity at large transverse momentum, $R_{p+Pb}(p_t \gg Q_s) \rightarrow 1$, as we shall discuss in detail later. While we presently lack a solid theoretical derivation for Eq. (10) we view it as a phenomenological way to ensure that the nuclear UGD is additive in the number of nucleons at small dipole sizes r or high intrinsic transverse momenta k_t .

In both cases, the total number of nucleons that overlap at a given transverse point, $N(\mathbf{R})$, is calculated via a simple geometric criterium:

$$N(\mathbf{R}) = \sum_{i=1}^A \Theta \left(\sqrt{\frac{\sigma_0}{\pi}} - |\mathbf{R} - \mathbf{r}_i| \right). \quad (11)$$

Some care must be exercised in choosing the transverse area σ_0 of the large- x partons of a nucleon. $Q_{s0,\text{proton}}$ corresponds to the density of large- x sources with $x > x_0$ and should therefore be energy independent (recoil of the sources is neglected in the small- x approximation). We therefore take $\sigma_0 \simeq 42$ mb to be given by the inelastic cross-section at $\sqrt{s} = 200$ GeV. However, σ_0 should not be confused with the energy dependent inelastic cross section $\sigma_{\text{in}}(s)$ of a nucleon which grows due to the emission of small- x gluons.

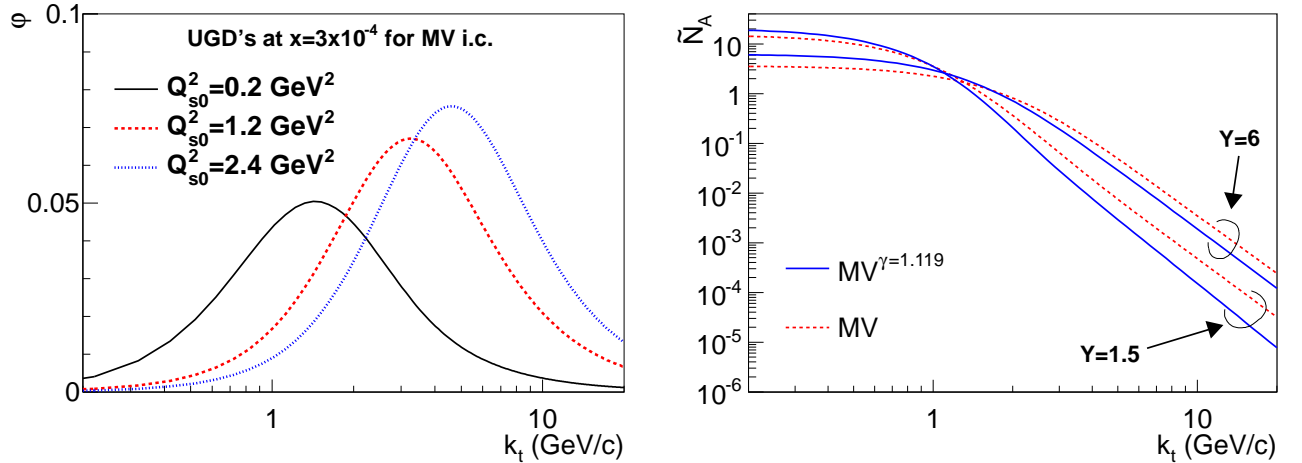


FIG. 1: Left: unintegrated gluon distributions $\varphi(k_t; x)$ for different values of the initial saturation scale evolved to $x = 3 \cdot 10^{-4}$ for MV initial conditions. Right: Fourier transform of the dipole scattering amplitude $\tilde{\mathcal{N}}_A(k; x)$ for a single nucleon and two different initial conditions: $MV^{\gamma=1.119}$ (solid) and MV (dashed) at rapidities $Y = \ln(x_0/x) = 1.5$ and 6.

In Fig. 1 we plot the UGD $\varphi(k_t; x)$ for three different initial saturation scales at $x = 3 \cdot 10^{-4}$ versus transverse momentum. The UGD corresponding to a single nucleon peaks at about $k_t \simeq 1$ GeV. The UGDs for larger Q_{s0}^2 illustrate the shift corresponding to a 6-nucleon and 12-nucleon target, respectively. These curves illustrate why one hopes that particle production at high energies and/or for heavy targets would become insensitive to physics at the confinement scale while instead being dominated by the semi-hard scale generated dynamically.

The plot on the right shows the different slopes for the two initial conditions ($MV^{\gamma=1.119}$ versus MV). The AAMQS UGD exhibits a substantial suppression of the high- k_t tail as compared to MV model initial conditions. At fixed k_t the suppression diminishes with evolution to higher rapidities. We shall show below that the AAMQS UGD provides a much better description of semi-hard p_t spectra in p+p collisions at high energies.

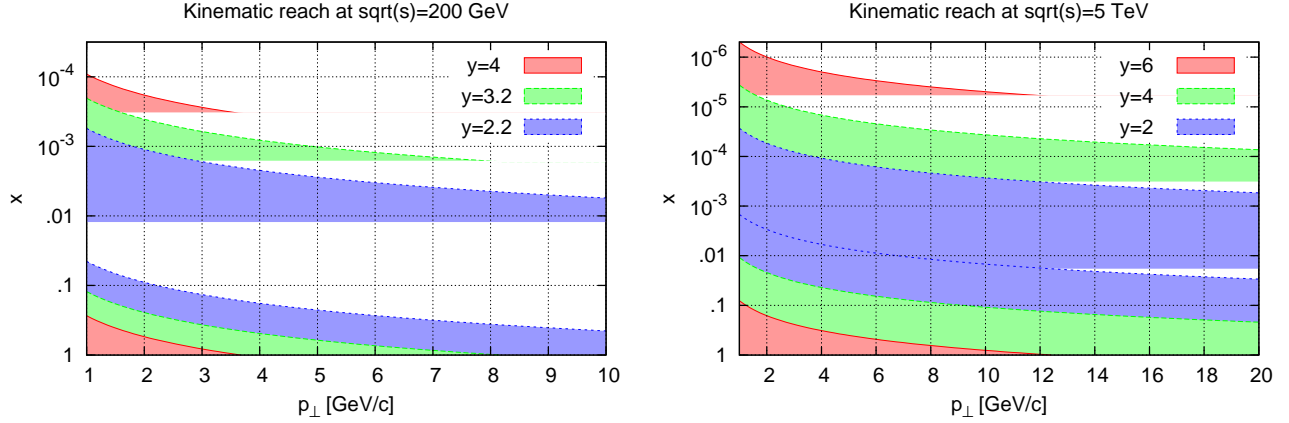


FIG. 2: Left: $x_{1,2}$ coverage at $y = 2.2, 3.2$ and 4.0 at RHIC energy $\sqrt{s} = 200$ GeV. Hadron p_{\perp} is limited to $p_T \lesssim 7.5$ (3.5) GeV/c at $y = 3.2$ (4.0) at RHIC. Right: $x_{1,2}$ coverage at $y = 4, 6$ at LHC energy.

III. PARTICLE PRODUCTION: k_t -FACTORIZATION AND *HYBRID* FORMALISMS

In this section we summarize how particle production is calculated from the UGDs described above. It is useful to first recall some elementary kinematics. For inclusive production of a single parton with transverse momentum p_t and rapidity y , *without* detection of the recoiling particle(s) in the opposite hemisphere, the $2 \rightarrow 1$ kinematics is such that projectile and target fields are probed at light cone momenta $x_{1,2} = (p_t/\sqrt{s})e^{\pm y}$. For the upcoming p+Pb run at the LHC we shall assume a collision energy of $\sqrt{s} = 5$ TeV. Hence, the production of particles with transverse momentum $p_t \lesssim 20$ GeV in the central rapidity region $|y| \lesssim 1$ probe both the projectile and target wave functions at small values of x below our initial condition at $x_0 = 0.01$ ⁵. In this case we shall use the so-called k_t -factorization approach. On the other hand, at more forward rapidities $y \gtrsim 2$, towards the proton fragmentation region, the momentum carried by the projectile parton grows large and so we shall resort to the hybrid formalism.

To outline the limits of applicability of our model let us first mention that in our terminology “small- x ” refers to $x \leq x_0 = 0.01$. This is the limit of applicability of the AAMQS fits to HERA data and coincides with parametric estimates for the validity of the CGC approach and of coherent interactions. To estimate the range of p_t where our calculations might be valid we again resort to the AAMQS fits: they start exhibiting some tension with the data when extended beyond $Q \sim 7 \div 10$ GeV. This may indicate failure of the CGC approach based on rcBK resummation for higher virtualities or transverse momenta. These limits of applicability are, of course, merely indicative, since one does not expect a sharp boundary but rather a smooth transition. The kinematic window accessible at RHIC and LHC, respectively, is illustrated in Fig. 2.

A. k_t -factorization

According to the k_t -factorization formalism [33], the number of gluons produced per unit rapidity at a transverse position \mathbf{R} in A+B collisions is given by

$$\frac{dN^{A+B \rightarrow g}}{dy d^2 p_t d^2 R} = \frac{1}{\sigma_s} \frac{d\sigma^{A+B \rightarrow g}}{dy d^2 p_t d^2 R}, \quad (12)$$

where σ_s represents the effective interaction area and $\sigma^{A+B \rightarrow g}$ is the cross section for inclusive gluon production:

$$\frac{d\sigma^{A+B \rightarrow g}}{dy d^2 p_t d^2 R} = K^k \frac{2}{C_F} \frac{1}{p_t^2} \int^{p_t} \frac{d^2 k_t}{4} \int d^2 b \alpha_s(Q) \varphi_P \left(\frac{|p_t + k_t|}{2}, x_1; b \right) \varphi_T \left(\frac{|p_t - k_t|}{2}, x_2; R - b \right). \quad (13)$$

⁵ A more precise estimate should consider the kinematic shift induced by the convolution of the primary produced parton with the fragmentation function, which is indeed taken into account in our calculation later on.

y and p_t are the rapidity and transverse momentum of the produced gluon, respectively, while $x_{1,2} = (p_t/\sqrt{s_{NN}})\exp(\pm y)$ and $C_F = (N_c^2 - 1)/2N_c$. As noted before, we assume that the local density in each nucleus is homogeneous over transverse distances of the order of the nucleon radius R_N . Thus, the b -integral in Eq. (13) yields a geometric factor proportional to the transverse “area” of a nucleon which cancels with a similar factor implicit in σ_s from Eq. (12), modulo subtleties in the definition of σ_s . Note, also, that (13) is symmetric under projectile \leftrightarrow target exchange if, simultaneously, one lets $y \rightarrow -y$.

Eq. (13) was written originally for fixed coupling. For consistency with our running coupling treatment of the small- x evolution of the UGDs, we allow the coupling to run with the momentum scale. The argument of the running coupling in Eq. (13) is chosen to be $Q = \max\{|p_t + k_t|/2, |p_t - k_t|/2\}$. However, we found rather weak sensitivity to the particular choice of scale because $\varphi \rightarrow 0$ as $k_t \rightarrow 0$ due to the saturation of $\mathcal{N}(r)$ at large dipole sizes r , see above. In principle one could improve on this educated guess by using the “running coupling k_t -factorization” formula derived recently in ref. [34]. Most importantly, the x -dependence of the dipole scattering amplitude obtained by solving the rcBK equation encodes all the collision energy and rapidity dependence of the gluon production formula Eq. (13).

The normalization factor K^k introduced in the k_t -factorization formula (13) above lumps together higher-order corrections, sea-quark contributions and, effectively, other dynamical effects not included in the CGC formulation. It can be fixed approximately from the charged particle transverse momentum distribution in p+p collisions at 7 TeV, see below. Although its precise value depends on the UGD and on the fragmentation function, we typically find $K^k \simeq 1.5 - 3$, which appears reasonable.

Eq. (13) is the starting point for all observables discussed below. In particular, the charged particle multiplicity and the transverse energy can be obtained by integrating over the transverse plane and p_t ,

$$\frac{dN_{\text{ch}}}{dy} = \frac{2}{3}\kappa_g \int d^2R \int d^2p_t \frac{dN^{A+B \rightarrow g}}{dy d^2p_t d^2R}, \quad (14)$$

$$\frac{dE_t}{dy} = \int d^2R \int d^2p_t p_t \frac{dN^{A+B \rightarrow g}}{dy d^2p_t d^2R}. \quad (15)$$

Note that a low- p_t cutoff is not required since the integration over k_t in (13) extends only up to p_t . The saturation of the gluon distribution functions guarantees that the dominant scale in the transverse momentum integrations is the saturation momentum. Similar to other CGC-based approaches, our Eq. (14) assumes that the total hadron multiplicity is proportional to the initial gluon multiplicity through an (energy and centrality independent) *gluon multiplication factor* κ_g ⁶. In order to reproduce both RHIC and LHC data on charged hadron multiplicities in heavy-ion collisions we fix it to be $\kappa_g \simeq 5$; small adjustments of this normalization factor may be required for p+p and p+Pb collisions as discussed below. This could be due to the fact that we here assume local rcBK evolution without explicit impact parameter dependence; further, due to our ignorance about how to hadronize the small- x gluons (which also determines the $y \rightarrow \eta$ Jacobian given below) etc. The precise value of κ_g does of course depend on the value of the K -factor which has been fixed independently since dN/dy only involves their product.

The upper limit in the integrals over the gluon transverse momentum in dN_{ch}/dy and dE_t/dy has been taken as $p_t^{\text{max}} = 12$ GeV; if the integrals are extended further then a slight adjustment of the normalization factors κ_g and K may be required. In order to compare our results for initial gluon production to the final state distributions of charged particles one has to translate the rapidity distributions into pseudo-rapidity distributions through the $y \rightarrow \eta$ Jacobian

$$\frac{dN_{\text{ch}}}{d\eta} = \frac{\cosh \eta}{\sqrt{\cosh^2 \eta + m^2/P^2}} \frac{dN_{\text{ch}}}{dy}, \quad \frac{dE_t}{d\eta} = \frac{\cosh \eta}{\sqrt{\cosh^2 \eta + m^2/P^2}} \frac{dE_t}{dy}, \quad (16)$$

with $y = \frac{1}{2} \ln(\sqrt{\cosh^2 \eta + m^2/P^2} + \sinh \eta)/(\sqrt{\cosh^2 \eta + m^2/P^2} - \sinh \eta)$. We assume that in this Jacobian $m = 350$ MeV and $P = 0.13$ GeV + 0.32 GeV $(\sqrt{s}/1 \text{ TeV})^{0.115}$ which leads to a reasonably good description of the pseudo-rapidity distribution of charged particles in p+p collisions at LHC energies, see below.

In turn, the single inclusive spectra at perturbatively large transverse momenta can be obtained by folding Eq. (13) for gluon production with the corresponding gluon fragmentation function:

$$\frac{dN^{A+B \rightarrow hX}}{dy d^2p_t} = \int d^2R \int \frac{dz}{z^2} D_g^h \left(z = \frac{p_t}{k_t}, Q \right) \frac{dN^{A+B \rightarrow g}}{dy d^2q_t d^2R}. \quad (17)$$

⁶ This factor does not enter Eq. (15) for the transverse energy because we assume that final-state gluon showering and hadronization conserves the energy per unit rapidity.

In (17) the integral over the hadron momentum fraction is restricted to $z \geq 0.05$ to avoid a violation of the momentum sum rule. The scale dependence of the FF of course emerges from a resummation of collinear singularities via the DGLAP equations and so its use in the k_\perp -factorization formula is not entirely justified.

B. Hybrid formalism

Moving away from central rapidity towards the projectile fragmentation region its wave function is probed at larger and larger momentum fraction x_1 which will eventually exceed $x = 0.01$. In this case the so-called hybrid formalism [30] is better suited for particle production. We shall employ the following expression for the differential cross section for production of a hadron with transverse momentum k and pseudorapidity⁷ η :

$$\frac{dN^{pA \rightarrow hX}}{d\eta d^2k} = K^h \left(\left[\frac{dN_h}{d\eta d^2k} \right]_{\text{el}} + \left[\frac{dN_h}{d\eta d^2k} \right]_{\text{inel}} \right) \quad (18)$$

where the subscripts *el* and *inel* stand for elastic and inelastic contributions⁸, respectively. We again allow for the presence of a K-factor, K^h , to absorb higher order corrections. The first term in Eq. (18), the elastic contribution, is given by [30]

$$\left[\frac{dN_h}{d\eta d^2k} \right]_{\text{el}} = \frac{1}{(2\pi)^2} \int_{x_F}^1 \frac{dz}{z^2} \left[\sum_q x_1 f_{q/p}(x_1, Q^2) \tilde{N}_F \left(x_2, \frac{p_t}{z} \right) D_{h/q}(z, Q^2) \right. \\ \left. + x_1 f_{g/p}(x_1, Q^2) \tilde{N}_A \left(x_2, \frac{p_t}{z} \right) D_{h/g}(z, Q^2) \right], \quad (19)$$

and corresponds to scattering of collinear partons from the projectile on the target. The $2 \rightarrow 1$ kinematics sets $x_{1,2} = (p_t/z\sqrt{s_{NN}}) \exp(\pm y)$ and $x_F \simeq (p_t/\sqrt{s_{NN}}) \exp \eta$. The projectile is described by standard collinear parton distribution functions (PDFs) but its partons acquire a large transverse momentum k due to (multiple) scattering from the small- x fields of the nucleus which are described by the corresponding UGDs in the adjoint or fundamental representation $\tilde{N}_{A(F)}$, see Eqs. (7). The hadronization of the scattered parton into a hadron is described by the usual fragmentation function (FF) of collinear factorization, $D_{h/j}$. Both the PDF and the FF are evaluated at the factorization scale Q . We shall explore the sensitivity to the choice of factorization scale by letting it vary within the range $Q = (k/2, 2k)$.

The inelastic term in Eq. (18) has been calculated recently in ref. [31]. It reads

$$\left[\frac{dN_h}{d\eta d^2k} \right]_{\text{inel}} = \frac{\alpha_s(Q)}{2\pi^2} \int_{x_F}^1 \frac{dz}{z^2} \frac{z^4}{k^4} \int^Q \frac{d^2q}{(2\pi)^2} q^2 \tilde{N}_F(x_2, q) x_1 \int_{x_1}^1 \frac{d\xi}{\xi} \sum_{i,j=q,\bar{q},g} w_{i/j}(\xi) P_{i/j}(\xi) f_j\left(\frac{x_1}{\xi}, Q^2\right) D_{h/j}(z, Q^2), \quad (20)$$

where $P_{i/j}$ are the LO DGLAP splitting functions for the different parton species $i, j = q, \bar{q}, g$. Note that endpoint singularities for $q \rightarrow q$ and $g \rightarrow g$ splitting are regulated via the usual “+ prescription”; therefore, the contribution from Eq. (20) is actually negative in parts of phase space. Explicit expressions for the weight functions $w_{i/j}(\xi)$ are given in Eqs. (74-77) of ref [31] and shall not be repeated here.

The inelastic term corresponds to an alternative channel for hard production: partons with high transverse momentum can occur in the wave function of the incoming proton due to large-angle radiation. Those may then scatter off the target with only a small momentum transfer to finally fragment into a high- p_t hadron. It should be noted that the inelastic term accounts for part of the full NLO corrections to the hybrid formalism. A calculation of the full NLO corrections to the hybrid formalism has been recently presented in [35, 36]. While a numerical implementation of the full NLO corrections would be necessary, such task is beyond the scope of this paper and we leave it for future work. The evaluation of the inelastic term in this work provides an estimate of the numerical importance of the full NLO corrections.

The inelastic contribution involves an additional power of the coupling α_s but also comes with a factor $\sim \log(k^2/Q_{s,T}^2)$ [31] and so is expected to be significant at high transverse momenta and not too forward rapidities, far from the kinematic boundary. These expectations have been first verified numerically in ref. [37]. Finally, we note that the scale for the running of the coupling in Eq. (20) cannot be determined from the calculation of ref. [31]

⁷ At forward rapidities the distinction between η and y becomes less relevant.

⁸ As a NLO contribution, the latter need not be positive definite, see below.

–a full NNLO calculation would be necessary to determine the scale for the running of the coupling at NLO– and should be considered as a free parameter. In order to assess the uncertainty related to the choice of scale for the coupling in the inelastic term, we shall consider two possibilities: assuming a constant value $\alpha_s = 0.1$ (similar to what was done in an earlier study [37]) or, alternatively, assuming one-loop running at the factorization scale Q by replacing $\alpha_s \rightarrow \alpha_s(Q)$ in Eq. (20).

IV. THE BASELINE: PROTON+PROTON COLLISIONS

In this section we first present our results for proton-proton collisions. We restrict to CM energies in the TeV regime so that the typical parton momentum fractions involved in semi-hard hadron production remain small. A good description of p_\perp distributions in p+p is of course required for a reliable calculation of the spectra in minimum-bias p+A collisions as well as for the R_{pA} nuclear modification factor. Furthermore, it is important to check consistency of the UGD in DIS and hadronic collisions. In what follows we shall use three different sets of fragmentation functions: LO-KKP [38] and DSS [39, 40] at LO and NLO, respectively.

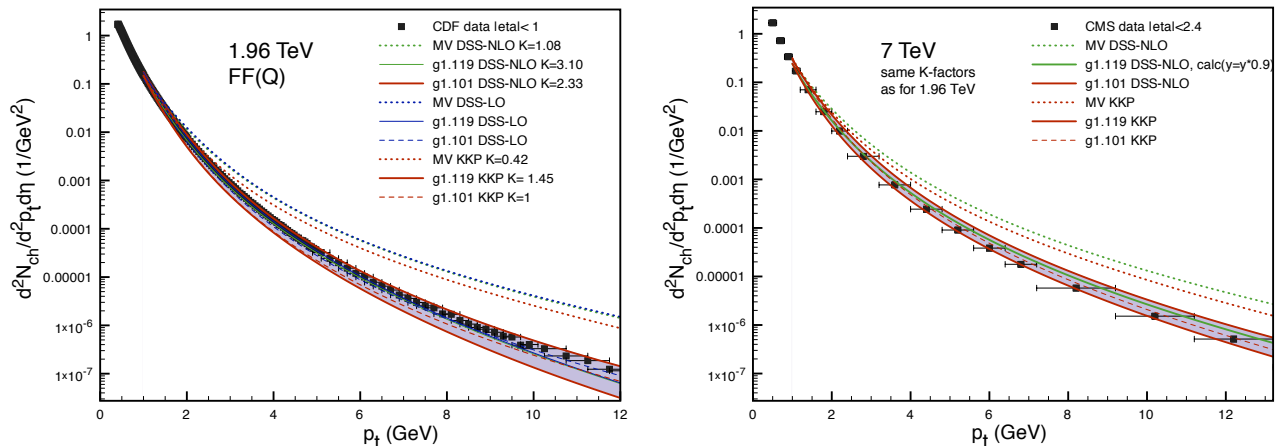


FIG. 3: Transverse momentum distribution of charged particles in the central region of p+p collisions at $\sqrt{s} = 1.96$ TeV (left), and p+p collisions at $\sqrt{s} = 7$ TeV (right). CDF and CMS data from refs. [41] and [42], respectively.

In Fig. 3 we show the transverse momentum distributions of charged particles in the regime of semi-hard p_t for inclusive p+p collisions at $\sqrt{s} = 1.96$ TeV and 7 TeV, respectively. We have tested various combinations of UGDs and FFs and in each case matched the K -factor to the data at $p_\perp = 1$ GeV.

First, we note that the UGD sets with the steeper initial gluon spectrum (UGD sets g1119 and g1101) lead to significantly better agreement with the data than the classical “MV model” initial condition with $\gamma = 1$; the latter leads to a p_\perp spectrum far outside the experimental error bars. This establishes consistency within our framework of the UGDs with DIS and hadron-hadron collisions, since those two sets provide a much better $\chi^2/d.o.f$ in fits to e+p data than the MV one. Recall, also, that in hadronic collisions $x \sim p_\perp$ for spectra at fixed rapidity. Hence, the shape of the spectra does provide a direct test of the rcBK evolution speed.

In Fig. 4 we check that changing the scale in the FF from $Q = p_\perp/2$ to $Q = p_\perp$ to $Q = 2p_\perp$ is mainly absorbed into a redefinition of the K -factor; in what follows we shall fix $Q = p_\perp$. Similarly, switching from DSS-LO to DSS-NLO FFs essentially leads to identical spectra once the K -factor is adjusted; see Fig. 3 (left). On the other hand, we obtain slightly harder spectra with DSS versus KKP fragmentation functions, as expected.

We now turn to the pseudo-rapidity dependence of p_\perp -integrated multiplicities. As already mentioned above, here we can not convolute the gluon spectrum with a fragmentation function. Instead, our crude “hadronization model” consist in assuming that on average over events the number of charged particles is proportional to the number of initially produced gluons. The number κ_g of final hadrons per initial gluon is a free parameter. Its precise value will depend on the UGD, on the assumed impact parameter distribution of valence charges in the nucleon, on the $\partial y/\partial \eta$ Jacobian and so on.

In Fig. 5 we compare to ALICE and CMS data from refs. [43–46]. For UGD 111 we have adjusted the normalization relative to that determined from Pb+Pb collisions by a factor of 1.24; the energy and rapidity dependence of $dN_{ch}/d\eta$ is consistent with the data. On the other hand, UGD 115 does not require any particular adjustment of normalization but appears to predict a slightly too steep energy dependence of the multiplicity and a narrower rapidity distribution (given our specific $\partial y/\partial \eta$ Jacobian).

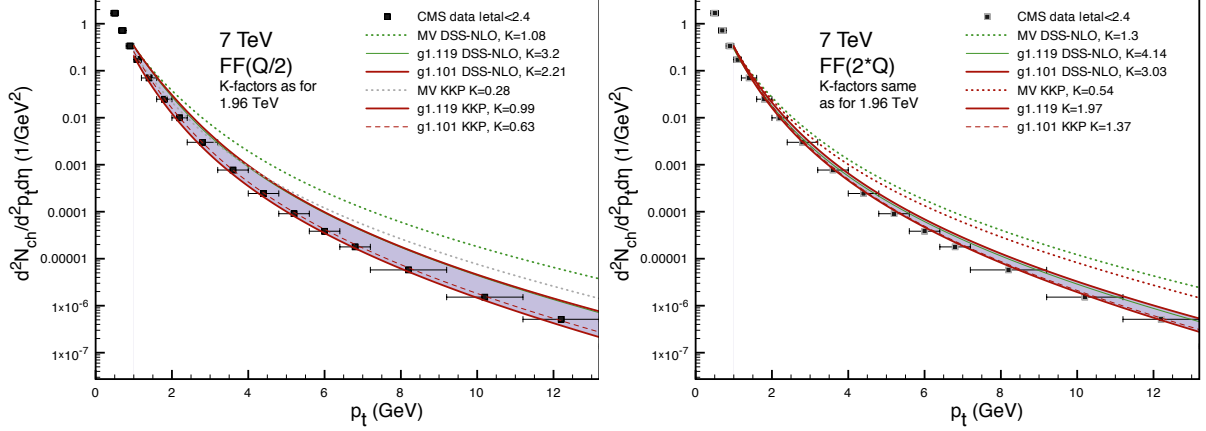


FIG. 4: Transverse momentum distribution of charged particles in the central region of p+p collisions at $\sqrt{s} = 7$ TeV. The scale in the FF is taken to be $Q = p_{\perp}/2$ (left) or $Q = 2p_{\perp}$ (right), respectively.

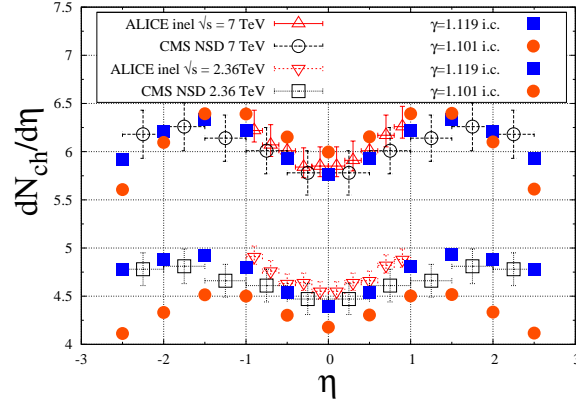


FIG. 5: Charged particle multiplicity as a function of pseudorapidity for p+p collisions at $\sqrt{s} = 2.36$ TeV and 7 TeV, respectively, for two different UGD sets (g1119 and g1101). ALICE and CMS data from refs. [43–46].

V. MULTIPLICITY IN P+PB COLLISIONS

In Fig. 6 we present our predictions for p_{\perp} -integrated multiplicities in minimum bias p+Pb collisions. According to our findings from above, for UGD set g1119 we use the exact same normalization as for Pb+Pb and p+p collisions. On the other hand, we had found that the UGD set g1101 requires a correction of +24% to reproduce the measured multiplicity in p+p collisions at 2360 and 7000 GeV. Accordingly, for this UGD set and min. bias p+Pb collisions we have increased by hand the normalization by +10% (relative to Pb+Pb). A prediction for the charged multiplicity for the UGD with MV-model i.c. ($\gamma = 1$) can be found in ref. [28]. We mention that the current results are similar to other predictions based on the idea of gluon saturation [47–49]. This illustrates that indeed the energy and system size dependence of the multiplicity is governed mainly by the dependence of the saturation scale Q_s on the target thickness and on x .

VI. SINGLE INCLUSIVE SPECTRA IN P+PB COLLISIONS

In this section we present single-inclusive charged hadron transverse momentum distributions for p+Pb collisions at $\sqrt{s} = 5$ TeV. For pseudo-rapidities near the central region, $|\eta| < 2$, the relevant light-cone momentum fractions in both projectile and target are comparable and small and so we use k_{\perp} factorization, section III A. We fix the K -factor to the value extracted from p+p collisions as described in the previous section. Our default fragmentation function is KKP-LO evaluated at the scale $Q^2 = k_t^2$.

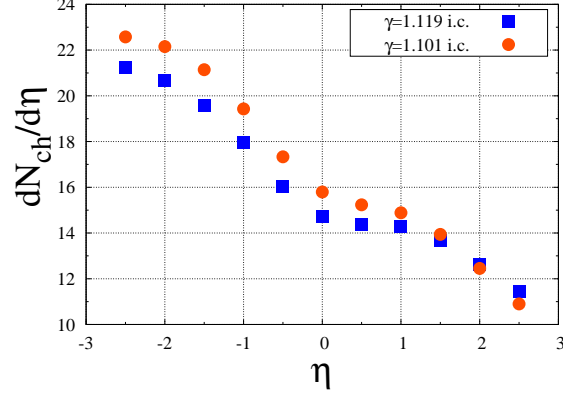


FIG. 6: Predicted pseudo-rapidity distribution of charged particles in minimum-bias p+Pb collisions at $\sqrt{s} = 5$ TeV for two different UGDs.

We shall also show the “nuclear modification factor” R_{p+Pb} defined as

$$R_{p+Pb}(p_\perp) \equiv \frac{1}{\langle N_{\text{coll}} \rangle} \frac{dN_{\text{ch}}^{p+Pb}/d\eta d^2p_\perp}{dN_{\text{ch}}^{p+p}/d\eta d^2p_\perp}, \quad (21)$$

where $\langle N_{\text{coll}} \rangle$ denotes the mean number of binary nucleon-nucleon collisions in a given centrality class; it is obtained from a standard MC Glauber model using an inelastic cross section of $\sigma_{\text{in}}(\sqrt{s} = 5 \text{ TeV}) = 67 \text{ mb}$. For minimum bias collisions this leads to $\langle N_{\text{coll}} \rangle \approx 7$.

To facilitate interpretation of the numerical results we shall not restrict to the AAMQS-like UGDs with $\gamma > 1$ initial condition but also show some curves obtained with the UGD with $\gamma = 1$ MV-model initial condition. We stress that although this UGD does not provide a good description of neither DIS data on protons nor of semi-hard p_t spectra in p+p collisions, it has not been directly tested against nuclear data yet and, therefore, remains a viable candidate for the initial condition for the evolution of nuclear wave functions.

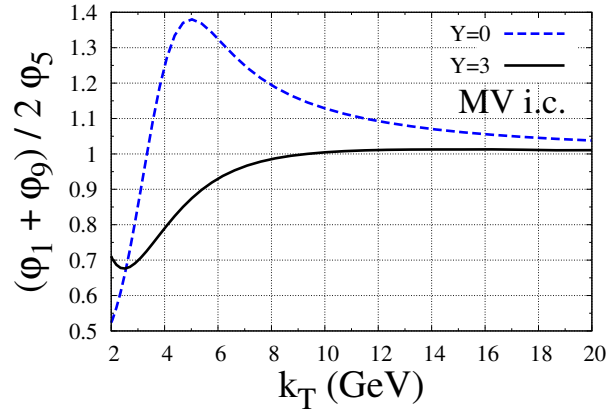


FIG. 7: Average of the gluon densities of a single nucleon and a nine nucleon target divided by the gluon density of a five nucleon target, for $Y = 0$ (MV i.c.) and $Y = 3$ (MV + rcBK), respectively.

We first illustrate the effects of quantum evolution and of fluctuations in the thickness of the target. Fig. 7 compares the average UGD of a 1-nucleon and 9-nucleon target to that of a 5-nucleon target. The MV initial condition at $Y = 0$ shows a strong suppression of this ratio at low intrinsic transverse momentum followed by a “Cronin-like” peak and an asymptotic approach to 1 from above (the leading higher-twist correction in the MV model is positive, $\sim +Q_s^4/k_T^6$; appendix B in ref. [50]). Neglecting fluctuations in the number of target nucleons could clearly distort the resulting R_{pA} ratio significantly. Actually, this could be origin of the slight differences between our predictions for R_{pPb} and those presented in [47] (shown in Fig. 11 below) with similar dynamical input

but where the nuclear geometry is treated in a mean field approach, hence neglecting fluctuations. Resummation of small- x quantum fluctuations removes the enhancement at intermediate k_T .

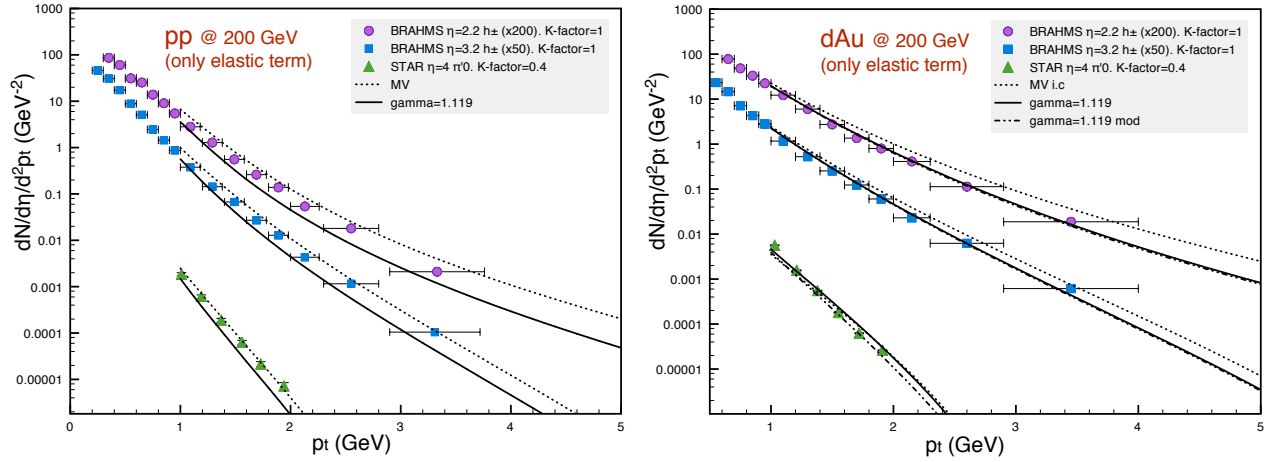


FIG. 8: Comparison of the rcBK-MC results obtained with only the elastic term of the hybrid formalism, Eq. (19), to the RHIC forward data on single inclusive charged hadron (BRAHMS data [51]) and neutral pion yields in p+p (left) and d+Au collisions (right). Solid lines correspond to the $\gamma = 1.119$ i.c., dashed-dotted to also $\gamma = 1.119$ i.c but using the prescription in Eq. (10) for the initial saturation scale. Dotted lines correspond to MV i.c.

In Fig. 8 we compare our results for single inclusive charged hadron (BRAHMS data [51]) and neutral pion (STAR data [52]) distributions measured in p+p and d+Au collisions at RHIC. In this figure we include only the elastic component of the hybrid formalism. In what follows we adopt the DSS-NLO fragmentation functions as the default ones for all the calculations performed within the hybrid formalism. Our results show a good agreement with data. However, the figure also illustrates that RHIC forward data does not constrain well the initial conditions for the evolution of nuclear wave functions: both the UGD MV and g1119 sets (using either the *natural*, Eq. (9), or the *modified*, Eq. (10), ansatz for the initial saturation scale at every point in the transverse plane) yield a comparably good description of data. This is due to the fact that transverse momentum distributions in the forward region do not probe the $k_T \gg Q_s$ tails of the UGDs.

Similar to previous phenomenological works, we found that no K-factors are needed to describe data at rapidities $\eta = 2.2$ and 3. However, STAR data at more forward rapidities can only be well described if a K-factor ≈ 0.4 is introduced. This may be an indication that large- x phenomena non included in the CGC may be relevant in the region close to the kinematic limit of phase space. Note, however, that the value of the K -factor depends significantly both on the UGD and on the FF.

In Fig. 9 we show the comparison to the same RHIC forward data, now also including the inelastic term in the hybrid formalism. We explore both fixed $\alpha_s = 0.1$ as well as one-loop running coupling at the scale Q . We observe that the effect of this additional term can be very large, especially at large transverse momentum. We note that, despite the fact that the coupling decreases with increasing transverse momentum, the running coupling prescription causes a larger effect than the fixed coupling one.

We observe that the inelastic term exhibits a harder p_T -dependence than the elastic contribution, and at some transverse momentum it overwhelms the elastic contribution. The crossing point depends on the particular choice of UGD. The effects from the inelastic corrections are stronger for the steeper g1119 initial conditions than for the MV ones over the entire range of transverse momentum shown in Fig. 9. Also, the importance of the inelastic term depends on the collision system or, equivalently, on the target saturation scale: it is stronger for p+p than for d+Au collisions. For p+p collisions in particular it appears that the present formalism does not provide a stable result as the inelastic correction overwhelms the leading elastic contribution already at moderate values of transverse momentum. This is not a completely unexpected result since, parametrically, the inelastic term is proportional to $\ln(p_t/Q_{st})$, with Q_{st} the target saturation scale, while the elastic term scales as $\ln(p_t/\Lambda_{QCD})$ (see discussion in [31]). Given the importance and magnitude of the inelastic term, our findings call for a complete phenomenological analysis of the full NLO corrections.

We now proceed to p+Pb collisions at LHC energy, $\sqrt{s} = 5$ TeV. In Figs. 10 and 11 we show our results for the single inclusive charged hadrons yields in p+p and minimum bias p+Pb collisions and the nuclear modification factor R_{p+Pb} for minimum bias collisions respectively. We compare also to R_{p+Pb} from collinear factorization using EPS09 nPDFs [53, 54] as well as to results from the “IP-sat” model and from an independent rcBK imple-

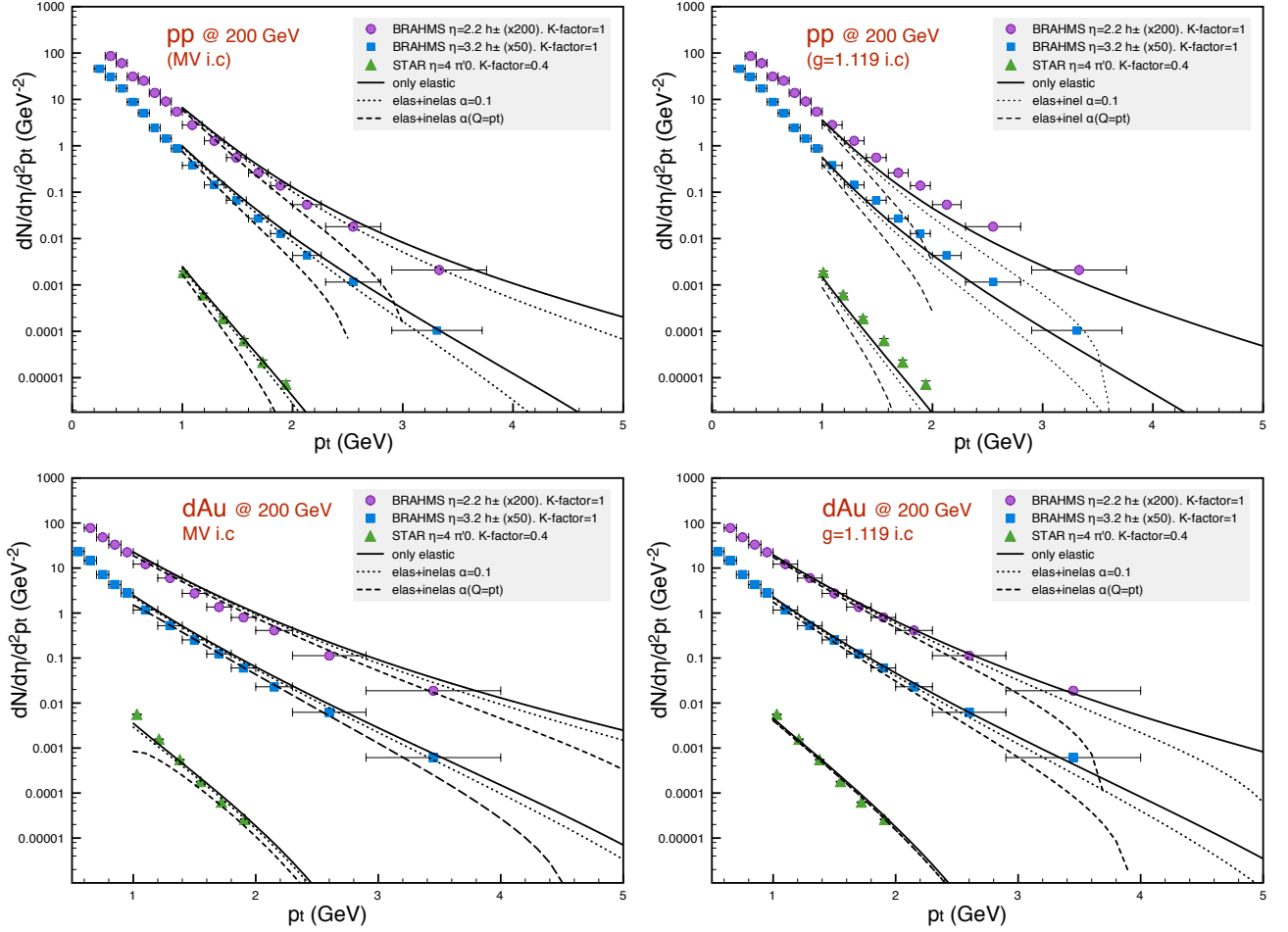


FIG. 9: Same as Fig. 8 but including the inelastic term in the hybrid formalism. Solid lines are the same as in Fig. 8. Dotted and dashed lines correspond to $\alpha_s = 0.1$ and $\alpha_s = \alpha_s(Q = p_t)$ in Eq. (20), respectively.

mentation⁹ [47].

Before discussing the results let us first explain the meaning of the rcBK-MC bands shown in Figs. 11-13: They comprise the results for R_{pPb} calculated according to Eq. (21) using the three UGD sets (g1119, g1101 and MV), the three kind of fragmentation functions (KKP-LO, DSS-LO and DSS-NLO) and the two possibilities to determine the initial saturation scale (*natural*, Eq. (9), or *modified*, Eq. (10)) considered throughout this work, always using the same configuration in the numerator $-p+Pb$ -spectrum- and denominator $-p+p$ -spectrum-. The upper limit of the bands correspond in all cases to R_{pPb} calculated with UGD set g1.119 together with the *natural* prescription for the initial saturation scale. The black solid line in the plots for $\eta = 0$ and 2 in Fig. 11 represents the upper limit of the band if only *modified* initial conditions are used (such distinction is not necessary for Figs. 12 and 13 since both cases are treated separately). For the results obtained within the k_t -factorization formalism the upper limit correspond to KKP-LO fragmentation functions, while for the results obtained within the hybrid formalism (both for *only elastic* and *elastic + inelastic* curves) the upper limit of the bands corresponds to DSS-NLO fragmentation functions. In turn, the lower limits of the bands correspond in all cases to UGD set MV and DSS-NLO fragmentation functions. The results for all other possible configurations – i.e. other UGDs and fragmentation functions and choice of *natural* or *modified* initial conditions– fall within the plotted bands; individual curves are not shown for clarity of the presentation.

⁹ To mention two differences to our work: ref. [47] uses a different fragmentation function and does not treat fluctuations of the nucleon configurations in the target. The predictions are not far apart but the difference illustrates the sensitivity of R_{pA} to such “details”.

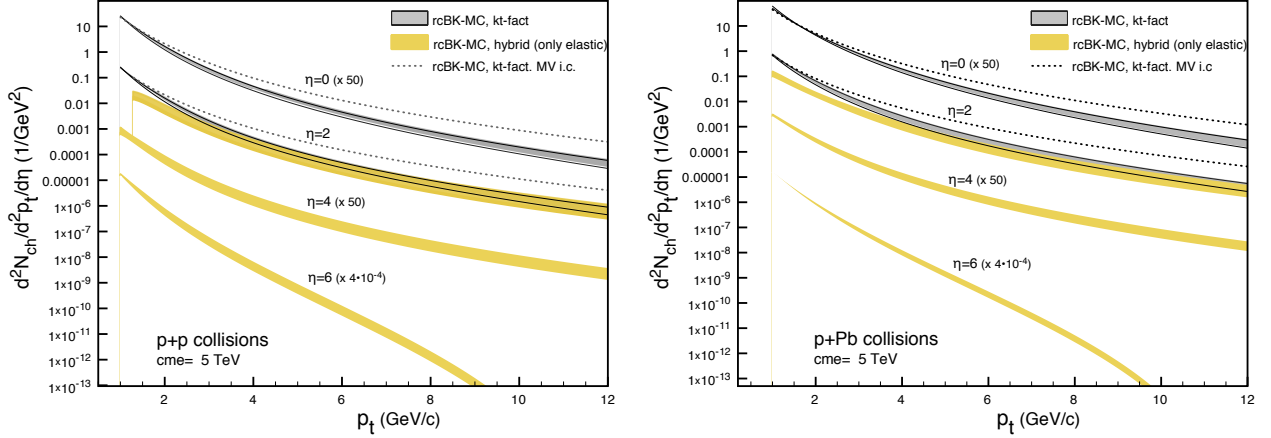


FIG. 10: Predictions for the single inclusive charged hadrons yields in p+p and minimum-bias p+Pb collisions at 5 TeV collision energy at rapidities 0, 2, 4 and 6. The grey bands at $y=0$ and 2 correspond to the rcBK-MC results using k_t -factorization, Eq. (13). Dotted lines correspond to MV i.c.. In turn, the yellow bands at $\eta = 2, 4$ and 6 have been obtained using the LO hybrid formalism including only the *elastic* term, Eq. (19). The overall normalization has been adjusted by a factor 50, 1, 0.02 and $4 \cdot 10^{-4}$ for rapidities 0, 2, 4 and 6 respectively to improve the visibility.

We observe a suppression of $R_{p+Pb} = 0.6 \pm 0.1$ at midrapidity and $p_t = 1$ GeV. Over the entire range of p_t shown in the figure, and for both UGDs, R_{p+Pb} decreases with increasing rapidity (towards the proton fragmentation region). This is consistent with expectations from non-linear evolution which suppresses additional gluon emissions in dense wave functions as compared to the dilute limit. However, we find that R_{p+Pb} increases with p_t and reaches, or even exceeds, unity for hadron transverse momenta of several GeV.

This is due to the following effects. First of all, the light-cone momentum fractions of gluons which contribute to hadron production at fixed rapidity increase proportional to p_t . This drives us closer to the initial condition which in fact exhibits an “anti-shadowing” *enhancement* of the UGD tail at high intrinsic transverse momentum¹⁰. This higher-twist “anti-shadowing” component is further enhanced by Glauber fluctuations in the Pb target since $\varphi(x, k_\perp)$ is not linear in the target thickness while $\langle N_{coll} \rangle$ in the denominator of Eq. (21) is. Nevertheless, it is remarkable that small- x quantum evolution in the rcBK approximation predicts a disappearance at LHC energies (and $\eta \geq 0$) of the clear Cronin peak observed so far in all proton-nucleus collisions at lower energies¹¹. Our results confirm earlier more schematic or qualitative predictions of this effect [56, 57]. Forthcoming LHC data will therefore provide a very important test for the evolution speed predicted by the running coupling BK equation.

It is also remarkable that at intermediate rapidities $\eta \approx 2$ the hybrid formalism with only the elastic term gives R_{pPb} systematically below the one from k_t -factorization. However, the inclusion of the inelastic term Eq. (20) in the calculations within the hybrid formalism tends to systematically increase R_{pPb} as compared to only the elastic component, bringing it closer to the R_{pPb} obtained from k_t -factorization. This effect is visible, in particular, at high transverse momentum, lifting R_{pPb} closer to unity. This confirms the expectation that higher-order and energy conservation corrections should bring p_t -spectra closer to the DGLAP limit at high transverse momenta, where gluon densities are smaller and non-linear corrections should be less relevant. However, as discussed previously, the precise quantitative effect of the inelastic term appears to depend quite strongly on the value of the strong coupling, preventing us to make precise quantitative predictions (only the results corresponding to $\alpha_s = 0.1$ are shown in Fig. (11); those corresponding to $\alpha_s = \alpha_s(Q)$ produce a much larger effect on R_{pPb}). Also, it is somewhat surprising that the effect is strongest at the most forward rapidities $\eta \approx 6$ and the highest transverse momentum (we cut off the curves corresponding to the inelastic term at $p_t \approx 8$ in this plot, since they grow very fast above unity for larger p_t). However, this region ($\eta \gtrsim 6$, $p_t \gtrsim 8$ GeV) is close to the kinematic limit at LHC energies (see Fig. 2). It could be that, similar to our discussion of forward RHIC data, the CGC formulation discussed in this work is not complete or inaccurate around the limit of phase space, hence the uncontrolled growth of R_{pPb} at the

¹⁰ Note, however, that the UGD with $\gamma = 1$ MV-model initial condition is very close to the EPS09 nPDF at high transverse momentum and $y = 0$. This indicates that for this UGD “anti-shadowing” is weak.

¹¹ Such a Cronin peak at 5 TeV is also predicted by some leading-twist shadowing models including parton intrinsic transverse momenta [55].

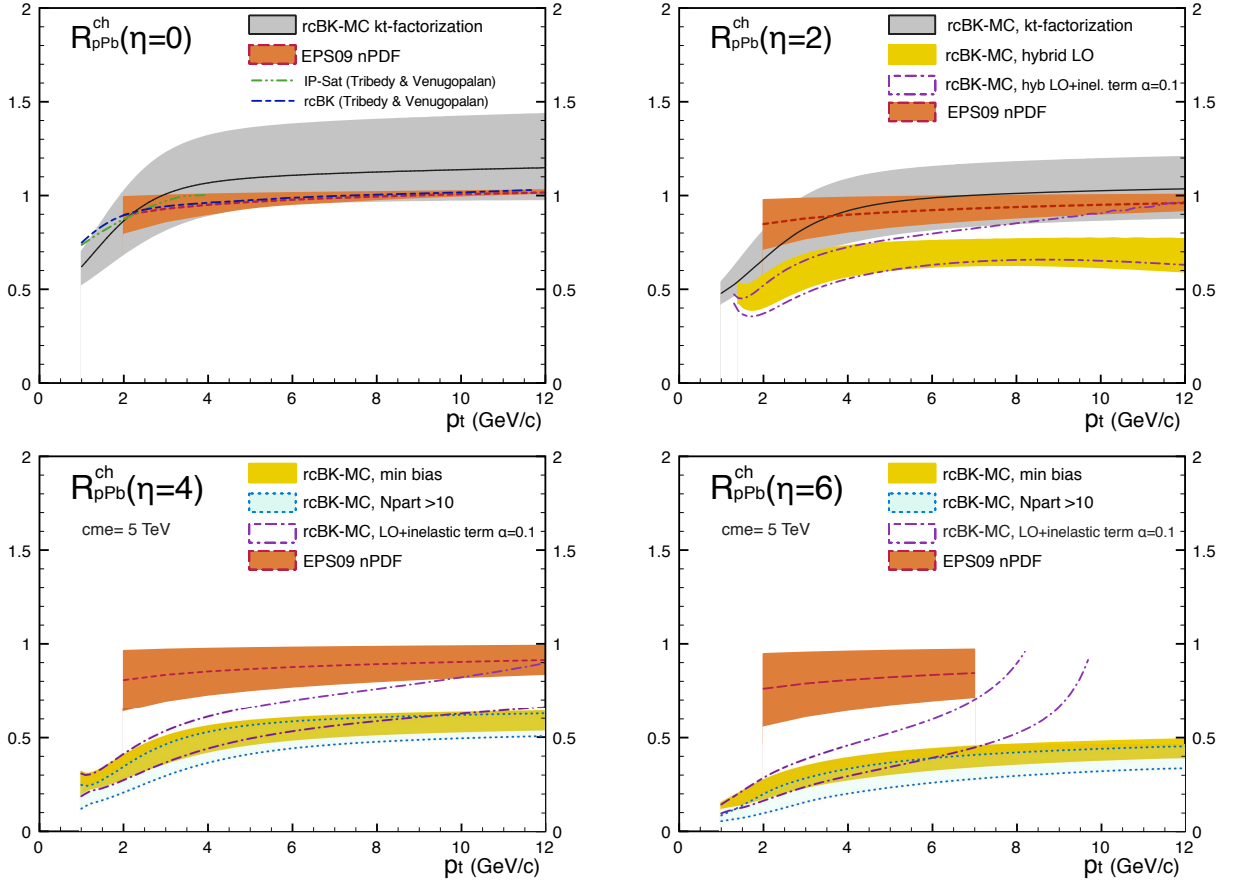


FIG. 11: The nuclear modification factor R_{p+Pb} for single inclusive charged hadrons in minimum-bias p+Pb collisions at 5 TeV collision energy at rapidities 0, 2, 4 and 6. The grey bands at $y=0$ and 2 correspond to the rcBK-MC results using kt-factorization, Eq. (13). In turn, the yellow bands at $\eta = 2, 4$ and 6 have been obtained using the LO hybrid formalism, Eq. (19), in minimum bias collisions. The blue bands between the dotted lines also correspond to LO hybrid results for collisions with a centrality cut $N_{part} > 10$. Finally the dashed dotted curves at $\eta = 2, 4$ and 6 correspond to minimum bias collisions calculated within the hybrid formalism incl. the inelastic term from Eq. (20) with $\alpha_s = 0.1$.

most forward rapidities.

In Fig. 12 we show R_{p+Pb} for two different centrality classes selected according to the number of participant nucleons¹². At $p_t = 1$ GeV we observe the expected pattern of stronger suppression (smaller R_{p+Pb}) for more central collisions. In the $N_{part} > 10$ centrality class suppression now persists up to $p_t = 2 - 3$ GeV.

For the UGD with $\gamma = 1$ MV-model initial condition (lower end of the bands in Fig. 12) one observes, generically, the expected pattern: i) at $y = 0$ there is suppression at low p_t while $R_{p+Pb} \rightarrow 1$ with increasing p_t as the rapidity evolution window shrinks; ii) there is slightly stronger suppression at low p_t for $N_{part} > 10$ central collisions while the centrality cut has very little effect at high p_t ; iii) the suppression increases with rapidity and $R_{p+Pb} < 1$ for all $p_t \lesssim 10$ GeV at $y = 2$.

The behavior of R_{p+Pb} with AAMQS UGDs ($\gamma = 1.119$ initial condition, upper end of the bands in Fig. 12) in central collisions is more intricate. At $p_t = 1$ GeV we still find the expected decrease of R_{p+Pb} both with centrality and rapidity. However, for $p_t \gtrsim 4$ GeV we find that R_{p+Pb} is very similar at $y = 0$ and $y = 2$. This UGD exhibits rather non-linear (in the valence charge density) anti-shadowing at high intrinsic k_t and so particle production at high p_t in p+Pb collisions is dominated by fluctuations corresponding to a high valence charge density in the Pb target (high N_{part}). This can be seen from the fact that at $y = 2$ and high p_t there is little difference between the minimum bias and $N_{part} > 10$ centrality classes.

¹² In p+A collisions it is not straightforward experimentally to perform centrality selection via impact parameter cuts. Also, because of large fluctuations impact parameter bins correspond to rather broad distributions of N_{part} .

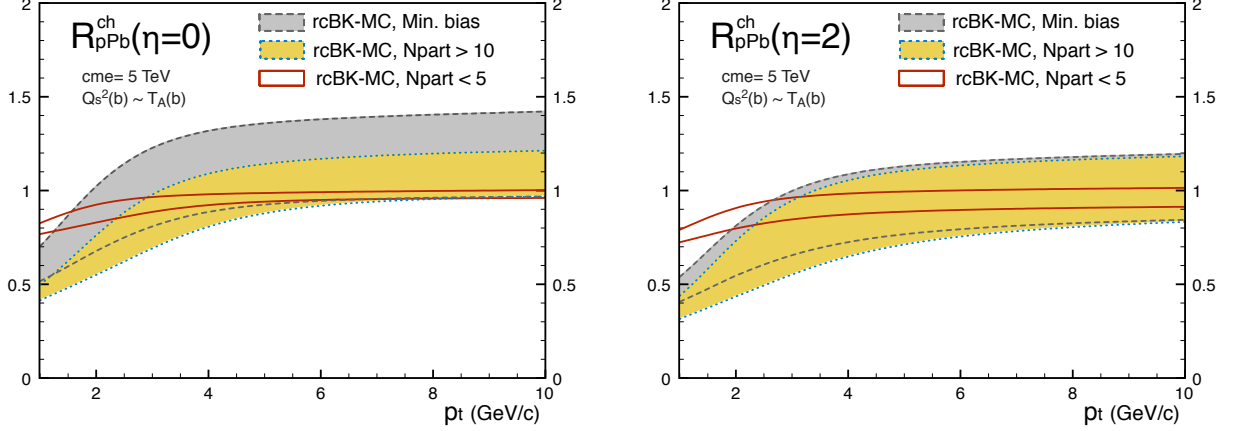


FIG. 12: Same as Fig. 11 for two different centrality classes. Here, for all curves the initial saturation momentum squared in the Pb target is taken to be proportional to the density of nucleons per unit transverse area in a given event, $Q_s^2(x_0; \mathbf{b}) \sim T_A(\mathbf{b})$, according to the *natural* prescription given by Eq. (9). Results in this plot have been calculated in the k_t -factorization formalism.

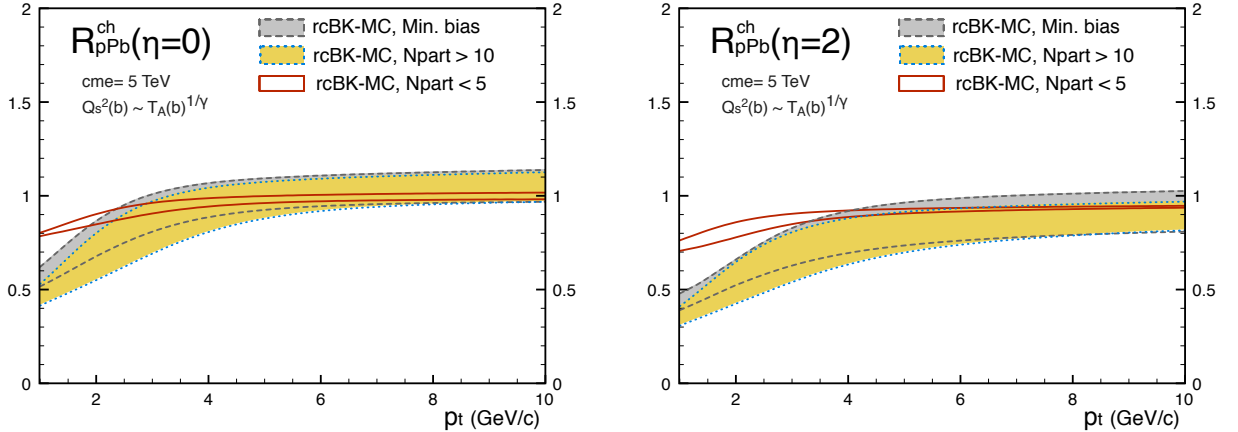


FIG. 13: Same as Fig. 12 but here the initial saturation momentum squared in the Pb target is taken as $Q_s^2(x_0; \mathbf{b}) \sim T_A^{1/\gamma}(\mathbf{b})$, according to the *modified* prescription given by Eq. (10). Results in this plot have been calculated in the k_t -factorization formalism.

In Fig. 13, finally, we show the nuclear modification factor for the UGDs with initial saturation momentum squared $Q_s^2(x_0; \mathbf{b}) \sim T_A^{1/\gamma}(\mathbf{b})$ which restores the $\mathcal{N}(r; x_0) \sim r^2$ behavior of the dipole scattering amplitude in the perturbative limit, $r Q_s(x_0) \ll 1$. This prescription for the initial saturation momentum reduces anti-shadowing at high intrinsic momenta. This leads to slightly lower values of R_{p+Pb} at high p_t than the AAMQS UGDs corresponding to $Q_s^2(x_0; \mathbf{b}) \sim T_A(\mathbf{b})$.

VII. MULTIPLICITY AND TRANSVERSE ENERGY IN PB+PB COLLISIONS

In this section we present the centrality dependence of the multiplicity and transverse energy in heavy-ion collisions at LHC energy¹³. This serves mainly as a rough check for the dependence of the saturation momentum on the thickness of a nucleus. We shall find that the present framework leads to a rather good description of the data. Nevertheless, we recall that we do not account for final-state effects such as entropy production; also, that our estimates rely on a crude “hadronization model” as well as on k_t -factorization which is not expected to be

¹³ Very similar results were previously presented in [28] (unpublished) before the corresponding data was available

very accurate for p_t integrated multiplicities in A+A collisions. That said, it is clearly justified to establish that the model is not in gross contradiction to basic features of heavy-ion data.

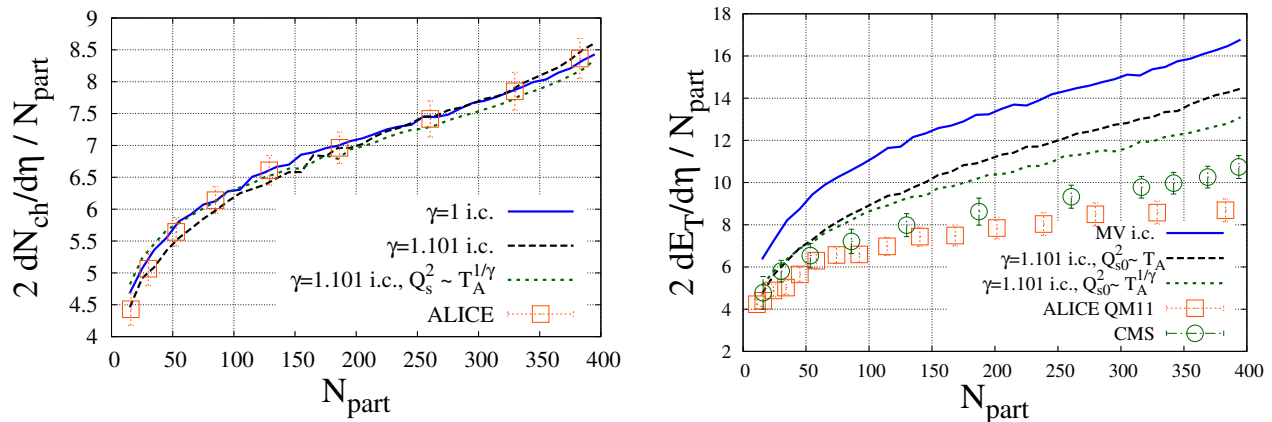


FIG. 14: Left: Centrality dependence of the charged particle multiplicity at midrapidity, $\eta = 0$; Pb+Pb collisions at 2760 GeV. We compare our calculation for two UGDs to data by the ALICE collaboration. Right: Centrality dependence of the transverse energy at $\eta = 0$.

We shall focus on the centrality dependence of the charged particle multiplicity at central rapidity, $\eta = 0$, which we determine along the lines described in section III A. The result is shown in Fig. 14 for the UGDs with MV-model ($\gamma = 1$) and AAMQS ($\gamma = 1.101$ and $Q_s^2(x_0) \sim T_A$ or $Q_s^2(x_0) \sim T_A^{1/\gamma}$) initial conditions. We use $K = 1.43$ for the former and $K = 2.0, 2.3$ for the latter. The number of final hadrons per gluon $\kappa_g = 5$ in all three cases.

All UGDs give a rather similar centrality dependence of the multiplicity which is in good agreement with ALICE data [58, 59]. On the other hand, they differ somewhat in their prediction for the transverse energy. This is of course due to the fact that the $\gamma = 1.1$ initial condition suppresses the high- k_t tail of the UGD¹⁴. With the K -factors mentioned above these UGDs match the measured E_t in peripheral collisions. This is a sensible result since one does not expect large final-state effects in very peripheral collisions. For the most central collisions the energy deposited initially at central rapidity is about 0.5% of the energy of the beams and exceeds the preliminary measurements by ALICE [60] and CMS [61] by roughly 50%. This leaves room for $-p \Delta V$ work due to longitudinal hydro expansion [62–64].

VIII. CONCLUSIONS

The upcoming p+Pb run at the LHC provides a new and unique opportunity to study the dynamics of very strong color fields in nuclei at high energies. The central question is whether QCD dynamically generates a semi-hard scale Q_s which dominates particle production and to test its dependence on the valence charge density (resp. the nuclear thickness) and on energy. In this paper we have provided phenomenological predictions and expectations to the best of our ability to model the large- x valence degrees of freedom paired with high-energy QCD evolution of the distribution of soft gluons in the rcBK approximation. As we have discussed at length throughout the paper, the CGC formalism at its present degree of accuracy is affected by sizable uncertainties. Some are due to the lack of quantitative control of higher order corrections to the formalism, while others are related to the lack of data constraining the non-perturbative parameters of the theory such as the initial conditions for the evolution or the impact parameter dependence of the UGDs. The forthcoming data will test whether the present formulation of the CGC effective theory is quantitatively accurate or not.

¹⁴ One should keep in mind though that our estimate of the initial transverse energy carries a significant uncertainty of at least $\pm 15\%$ related to our choice of K -factor; it is *not* determined accurately by the multiplicity since the latter involves only the product of K -factor and gluon \rightarrow hadron multiplication factor κ_g .

Acknowledgements

The research of J. L. Albacete is supported by a fellowship from the Théorie LHC France initiative funded by the IN2P3. A.D. is supported by the DOE Office of Nuclear Physics through Grant No. DE-FG02-09ER41620 and by The City University of New York through the PSC-CUNY Research Award Program, grant 65041-0043. H.F. and Y.N. were supported in part by Grant-in-Aid for Scientific Research (B) 22340064. We thank Paloma Quiroga-Arias for providing us with the EPS09 results shown in Fig. 8 and also P. Tribedy and R. Venugopalan for providing us with their CGC-predictions shown in Fig. 8 (top-left). Finally we thank A. Kovner and B. W. Xiao for very informative discussions on the comparison of the inelastic and NLO corrections to the hybrid formalism.

-
- [1] C. Salgado, J. Alvarez-Muniz, F. Arleo, N. Armesto, M. Botje, et al., Proton-Nucleus Collisions at the LHC: Scientific Opportunities and Requirements, *J.Phys.G* G39 (2012) 015010. arXiv:1105.3919, doi:10.1088/0954-3899/39/1/015010.
 - [2] A. H. Mueller, Parton saturation at small x and in large nuclei, *Nucl. Phys.* B558 (1999) 285–303. arXiv:hep-ph/9904404.
 - [3] H. Weigert, Evolution at small x : The color glass condensate, *Prog. Part. Nucl. Phys.* 55 (2005) 461–565. arXiv:hep-ph/0501087.
 - [4] F. Gelis, E. Iancu, J. Jalilian-Marian, R. Venugopalan, The Color Glass Condensate, *Ann.Rev.Nucl.Part.Sci.* 60 (2010) 463–489. arXiv:1002.0333, doi:10.1146/annurev.nucl.010909.083629.
 - [5] L. D. McLerran, R. Venugopalan, Computing quark and gluon distribution functions for very large nuclei, *Phys. Rev. D* 49 (1994) 2233–2241. arXiv:hep-ph/9309289.
 - [6] L. D. McLerran, R. Venugopalan, Gluon distribution functions for very large nuclei at small transverse momentum, *Phys. Rev. D* 49 (1994) 3352–3355. arXiv:hep-ph/9311205.
 - [7] I. Balitsky, Operator expansion for high-energy scattering, *Nucl. Phys.* B463 (1996) 99–160. arXiv:hep-ph/9509348.
 - [8] Y. V. Kovchegov, Small- x F_2 structure function of a nucleus including multiple pomeron exchanges, *Phys. Rev. D* 60 (1999) 034008. arXiv:hep-ph/9901281.
 - [9] Y. Kovchegov, H. Weigert, Triumvirate of Running Couplings in Small- x Evolution, *Nucl. Phys. A* 784 (2007) 188–226. arXiv:hep-ph/0609090.
 - [10] I. I. Balitsky, Quark Contribution to the Small- x Evolution of Color Dipole, *Phys. Rev. D* 75 (2007) 014001. arXiv:hep-ph/0609105.
 - [11] E. Gardi, J. Kuokkanen, K. Rummukainen, H. Weigert, Running coupling and power corrections in nonlinear evolution at the high-energy limit, *Nucl. Phys. A* 784 (2007) 282–340. arXiv:hep-ph/0609087.
 - [12] I. Balitsky, G. A. Chirilli, Next-to-leading order evolution of color dipoles, *Phys. Rev. D* 77 (2008) 014019. arXiv:0710.4330, doi:10.1103/PhysRevD.77.014019.
 - [13] J. L. Albacete, Y. V. Kovchegov, Solving high energy evolution equation including running coupling corrections, *Phys. Rev. D* 75 (2007) 125021. arXiv:arXiv:0704.0612 [hep-ph].
 - [14] J. L. Albacete, N. Armesto, J. G. Milhano, C. A. Salgado, Non-linear QCD meets data: A global analysis of lepton- proton scattering with running coupling BK evolution, *Phys. Rev. D* 80 (2009) 034031. arXiv:0902.1112, doi:10.1103/PhysRevD.80.034031.
 - [15] J. L. Albacete, N. Armesto, J. G. Milhano, P. Quiroga Arias, C. A. Salgado, AAMQS: A non-linear QCD analysis of new HERA data at small- x including heavy quarks, *Eur.Phys.J. C* 71 (2011) 1705, * Temporary entry *. arXiv:1012.4408, doi:10.1140/epjc/s10052-011-1705-3.
 - [16] J. Albacete, J. Milhano, P. Quiroga-Arias, J. Rojo, Linear vs non-linear QCD evolution: from HERA data to LHC phenomenology arXiv:1203.1043.
 - [17] J. Kuokkanen, K. Rummukainen, H. Weigert, HERA-data in the light of small x evolution with state of the art NLO input, *Nucl.Phys. A* 875 (2012) 29–93. arXiv:1108.1867.
 - [18] J. L. Albacete, C. Marquet, Single Inclusive Hadron Production at RHIC and the LHC from the Color Glass Condensate, *Phys. Lett. B* 687 (2010) 174–179. arXiv:1001.1378, doi:10.1016/j.physletb.2010.02.073.
 - [19] H. Fujii, K. Itakura, Y. Kitadono, Y. Nara, Forward particle productions at RHIC and the LHC from CGC within local rcBK evolution, *J.Phys.G* G38 (2011) 124125. arXiv:1107.1333, doi:10.1088/0954-3899/38/12/124125.
 - [20] H. Fujii, K. Itakura and Y. Nara, Forward hadron productions at collider energies in CGC framework, *Prog.Theor.Phys.Suppl.* 193 (2012) 216. doi:10.1143/PTPS.193.216.
 - [21] B. Z. Kopeliovich, J. Nemchik, I. K. Potashnikova, M. B. Johnson, I. Schmidt, Breakdown of QCD factorization at large Feynman x , *Phys. Rev. C* 72 (2005) 054606. arXiv:hep-ph/0501260, doi:10.1103/PhysRevC.72.054606.
 - [22] C. Marquet, Forward inclusive dijet production and azimuthal correlations in pA collisions, *Nucl. Phys. A* 796 (2007) 41–60. arXiv:0708.0231, doi:10.1016/j.nuclphysa.2007.09.001.
 - [23] J. L. Albacete, C. Marquet, Azimuthal correlations of forward di-hadrons in d+Au collisions at RHIC in the Color Glass Condensate, *Phys.Rev.Lett.* 105 (2010) 162301. arXiv:1005.4065, doi:10.1103/PhysRevLett.105.162301.
 - [24] A. Stasto, B.-W. Xiao, F. Yuan, Back-to-Back Correlations of Di-hadrons in dAu Collisions at RHIC arXiv:1109.1817.
 - [25] Z.-B. Kang, I. Vitev, H. Xing, Dihadron momentum imbalance and correlations in d+Au collisions, *Phys.Rev. D* 85

- (2012) 054024. arXiv:1112.6021, doi:10.1103/PhysRevD.85.054024.
- [26] M. Strikman, W. Vogelsang, Multiple parton interactions and forward double pion production in pp and dA scattering, *Phys. Rev. D* **83** (2011) 034029. arXiv:1009.6123, doi:10.1103/PhysRevD.83.034029.
 - [27] N. Armesto, (ed.), et al., Heavy Ion Collisions at the LHC - Last Call for Predictions, *J. Phys. G* **35** (2008) 054001. arXiv:0711.0974, doi:10.1088/0954-3899/35/5/054001.
 - [28] J. L. Albacete, A. Dumitru, A model for gluon production in heavy-ion collisions at the LHC with rcBK unintegrated gluon densities arXiv:1011.5161.
 - [29] H.-J. Drescher, Y. Nara, Eccentricity fluctuations from the Color Glass Condensate at RHIC and LHC, *Phys. Rev. C* **76** (2007) 041903. arXiv:0707.0249, doi:10.1103/PhysRevC.76.041903.
 - [30] A. Dumitru, A. Hayashigaki, J. Jalilian-Marian, The color glass condensate and hadron production in the forward region, *Nucl. Phys. A* **765** (2006) 464–482. arXiv:hep-ph/0506308, doi:10.1016/j.nuclphysa.2005.11.014.
 - [31] T. Altinoluk, A. Kovner, Particle Production at High Energy and Large Transverse Momentum - 'The Hybrid Formalism' Revisited, *Phys. Rev. D* **83** (2011) 105004. arXiv:1102.5327, doi:10.1103/PhysRevD.83.105004.
 - [32] A. Dumitru, E. Petreska, Initial conditions for dipole evolution beyond the McLerran-Venugopalan model, *Nucl. Phys. A* **879** (2012) 59–76. arXiv:1112.4760, doi:10.1016/j.nuclphysa.2012.02.006.
 - [33] Y. V. Kovchegov, K. Tuchin, Inclusive gluon production in dis at high parton density, *Phys. Rev. D* **65** (2002) 074026. arXiv:hep-ph/0111362.
 - [34] W. Horowitz, Y. V. Kovchegov, Running Coupling Corrections to High Energy Inclusive Gluon Production, *Nucl. Phys. A* **849** (2011) 72–97. arXiv:1009.0545, doi:10.1016/j.nuclphysa.2010.10.014.
 - [35] G. A. Chirilli, B.-W. Xiao, F. Yuan, One-loop Factorization for Inclusive Hadron Production in pA Collisions in the Saturation Formalism, *Phys. Rev. Lett.* **108** (2012) 122301. arXiv:1112.1061, doi:10.1103/PhysRevLett.108.122301.
 - [36] G. A. Chirilli, B.-W. Xiao, F. Yuan, Inclusive Hadron Productions in pA Collisions arXiv:1203.6139.
 - [37] J. Jalilian-Marian, A. H. Rezaeian, Hadron production in pA collisions at the LHC from the Color Glass Condensate, *Phys. Rev. D* **85** (2012) 014017. arXiv:1110.2810, doi:10.1103/PhysRevD.85.014017.
 - [38] B. A. Kniehl, G. Kramer, B. Potter, Fragmentation functions for pions, kaons, and protons at next-to-leading order, *Nucl. Phys. B* **582** (2000) 514–536. arXiv:hep-ph/0010289, doi:10.1016/S0550-3213(00)00303-5.
 - [39] D. de Florian, R. Sassot, M. Stratmann, Global analysis of fragmentation functions for pions and kaons and their uncertainties, *Phys. Rev. D* **75** (2007) 114010. arXiv:hep-ph/0703242, doi:10.1103/PhysRevD.75.114010.
 - [40] D. de Florian, R. Sassot, M. Stratmann, Global analysis of fragmentation functions for protons and charged hadrons, *Phys. Rev. D* **76** (2007) 074033. arXiv:0707.1506, doi:10.1103/PhysRevD.76.074033.
 - [41] T. Aaltonen, et al., Measurement of Particle Production and Inclusive Differential Cross Sections in p anti- p Collisions at $s^{1/2} = 1.96$ -TeV, *Phys. Rev. D* **79** (2009) 112005. arXiv:0904.1098, doi:10.1103/PhysRevD.82.119903, 10.1103/PhysRevD.79.112005.
 - [42] V. Khachatryan, et al., Transverse-momentum and pseudorapidity distributions of charged hadrons in pp collisions at $\sqrt{s} = 7$ TeV, *Phys. Rev. Lett.* **105** (2010) 022002. arXiv:1005.3299, doi:10.1103/PhysRevLett.105.022002.
 - [43] K. Aamodt, et al., Charged-particle multiplicity measurement in proton-proton collisions at $\sqrt{s} = 0.9$ and 2.36 TeV with ALICE at LHC, *Eur. Phys. J. C* **68** (2010) 89–108. arXiv:1004.3034, doi:10.1140/epjc/s10052-010-1339-x.
 - [44] K. Aamodt, et al., Charged-particle multiplicity measurement in proton-proton collisions at $\sqrt{s} = 7$ TeV with ALICE at LHC, *Eur. Phys. J. C* **68** (2010) 345–354. arXiv:1004.3514, doi:10.1140/epjc/s10052-010-1350-2.
 - [45] V. Khachatryan, et al., Transverse momentum and pseudorapidity distributions of charged hadrons in pp collisions at $\sqrt{s} = 0.9$ and 2.36 TeV, *JHEP* **1002** (2010) 041. arXiv:1002.0621, doi:10.1007/JHEP02(2010)041.
 - [46] V. Khachatryan, et al., Charged particle multiplicities in pp interactions at $\sqrt{s} = 0.9$, 2.36, and 7 TeV, *JHEP* **1101** (2011) 079. arXiv:1011.5531, doi:10.1007/JHEP01(2011)079.
 - [47] P. Tribedy, R. Venugopalan, QCD saturation at the LHC: comparisons of models to p+p and A+A data and predictions for p+Pb collisions, *Phys. Lett. B* **710** (2012) 125–133. arXiv:1112.2445, doi:10.1016/j.physletb.2012.02.047.
 - [48] A. H. Rezaeian, Charged particle multiplicities in pA interactions at the LHC from the Color Glass Condensate, *Phys. Rev. D* **85** (2012) 014028. arXiv:1111.2312, doi:10.1103/PhysRevD.85.014028.
 - [49] A. Dumitru, D. E. Kharzeev, E. M. Levin, Y. Nara, Gluon Saturation in pA Collisions at the LHC: KLN Model Predictions For Hadron Multiplicities, *Phys. Rev. C* **85** (2012) 044920. arXiv:1111.3031, doi:10.1103/PhysRevC.85.044920.
 - [50] F. Gelis, A. Peshier, Probing colored glass via q anti- q photoproduction, *Nucl. Phys. A* **697** (2002) 879–901. arXiv:hep-ph/0107142, doi:10.1016/S0375-9474(01)01264-7.
 - [51] I. Arsene, et al., On the evolution of the nuclear modification factors with rapidity and centrality in d + Au collisions at $s(NN)^{1/2} = 200$ -GeV, *Phys. Rev. Lett.* **93** (2004) 242303. arXiv:nucl-ex/0403005, doi:10.1103/PhysRevLett.93.242303.
 - [52] J. Adams, et al., Forward neutral pion production in p+p and d+Au collisions at $s(NN)^{1/2} = 200$ -GeV, *Phys. Rev. Lett.* **97** (2006) 152302. arXiv:nucl-ex/0602011, doi:10.1103/PhysRevLett.97.152302.
 - [53] K. J. Eskola, H. Paukkunen, C. A. Salgado, EPS09 - a New Generation of NLO and LO Nuclear Parton Distribution Functions, *JHEP* **04** (2009) 065. arXiv:0902.4154, doi:10.1088/1126-6708/2009/04/065.
 - [54] P. Quiroga-Arias, J. G. Milhano, U. A. Wiedemann, Testing nuclear parton distributions with pA collisions at the TeV scale, *Phys. Rev. C* **82** (2010) 034903. arXiv:1002.2537, doi:10.1103/PhysRevC.82.034903.
 - [55] R. Xu, W.-T. Deng, X.-N. Wang, Suppression of high P_T hadron spectra in $p + A$ collisions arXiv:1207.6836.
 - [56] J. L. Albacete, N. Armesto, A. Kovner, C. A. Salgado, U. A. Wiedemann, Energy dependence of the Cronin effect from nonlinear QCD evolution, *Phys. Rev. Lett.* **92** (2004) 082001. arXiv:hep-ph/0307179,

doi:10.1103/PhysRevLett.92.082001.

- [57] D. Kharzeev, Y. V. Kovchegov, K. Tuchin, Cronin effect and high $p(T)$ suppression in pA collisions, Phys.Rev. D68 (2003) 094013. arXiv:hep-ph/0307037, doi:10.1103/PhysRevD.68.094013.
- [58] B. Abelev, et al., Charged-particle multiplicity density at mid-rapidity in central Pb-Pb collisions at $\sqrt{s_{NN}} = 2.76$ TeV, Phys. Rev. Lett. 105 (2010) 252301. arXiv:1011.3916.
- [59] K. Aamodt, et al., Centrality dependence of the charged-particle multiplicity density at mid-rapidity in Pb-Pb collisions at $\sqrt{s_{NN}} = 2.76$ TeV, Phys.Rev.Lett. 106 (2011) 032301. arXiv:1012.1657, doi:10.1103/PhysRevLett.106.032301.
- [60] A. Toia, Bulk Properties of Pb-Pb collisions at $\sqrt{s_{NN}} = 2.76$ TeV measured by ALICE, J.Phys.G G38 (2011) 124007. arXiv:1107.1973, doi:10.1088/0954-3899/38/12/124007.
- [61] S. Chatrchyan, et al., Measurement of the pseudorapidity and centrality dependence of the transverse energy density in PbPb collisions at $\sqrt{s_{NN}} = 2.76$ TeV arXiv:1205.2488.
- [62] M. Gyulassy, Y. Pang, B. Zhang, Transverse energy evolution as a test of parton cascade models, Nucl.Phys. A626 (1997) 999–1018. arXiv:nucl-th/9709025, doi:10.1016/S0375-9474(97)00604-0.
- [63] K. Eskola, K. Kajantie, P. Ruuskanen, K. Tuominen, Scaling of transverse energies and multiplicities with atomic number and energy in ultrarelativistic nuclear collisions, Nucl.Phys. B570 (2000) 379–389. arXiv:hep-ph/9909456, doi:10.1016/S0550-3213(99)00720-8.
- [64] A. Dumitru, M. Gyulassy, The effective pressure of a saturated gluon plasma, Phys.Lett. B494 (2000) 215–220. arXiv:hep-ph/0006257, doi:10.1016/S0370-2693(00)01174-6.